

Bio-inspired Artemether loaded Human Serum Albumin Nanoparticles for Effective Control of Malaria-infected Erythrocytes

Aditi A. Sidhaye,¹ Kanchan C. Bhuran,¹ Sneha Zambare,¹ Munna Abubaker,² Niroshini Nirmalan² and Kamalinder K. Singh ^{1,3*}

¹*C. U. Shah College of Pharmacy, S.N. D. T. Women's University, Santacruz (W), Mumbai 400049, India*

²*School of Environment and Life Sciences, The University of Salford, Manchester, M5 4WT, United Kingdom*

³*School of Pharmacy and Biomedical Sciences, University of Central Lancashire, Preston, PR1 2HE, United Kingdom*

*To whom correspondence should be addressed:

Kamalinder K. Singh
School of Pharmacy and Biomedical Sciences,
University of Central Lancashire,
Preston, PR1 2HE, United Kingdom

Abstract

Background: The intra-erythrocytic development of the malarial parasite is dependent on active uptake of nutrients, including human serum albumin(HSA), into parasitized erythrocytes(pRBCs). We have designed HSA-based nanoparticles as a potential drug-delivery option for antimalarials. **Methods:** Artemether-loaded nanoparticles(AAN) were designed and antimalarial activity evaluated *in-vitro/in-vivo* using *Plasmodium falciparum/Plasmodium berghei* species, respectively. **Results:** Selective internalisation of AAN into *Plasmodium*-infected RBCs in preference to healthy erythrocytes was observed using confocal-imaging. *In-vitro* studies showed 50% dose reduction for AAN as compared to drug-only controls to achieve IC₅₀ levels of inhibition. The nanoparticles exhibited 2-fold higher peak drug concentrations in RBCs with antimalarial activity at 50% of therapeutic doses in *P.bergei*-infected mice. **Conclusion:** HSA-based nanoparticles offer safe and effective approach for selective targeting of antimalarial drugs.

Key words: Human serum albumin nanoparticles, artemether, malaria, parasitized RBCs

1. Introduction

Malaria is a global health priority with more than 3 billion people at risk [1]. Effective treatment of malaria is hampered by the development and rapid spread of resistance to all known classes of antimalarials. Furthermore, the non-specific targeting of intracellular parasites result in high doses of therapeutic agents being used with higher incidence of related toxicities. Upon invasion by the malaria parasite, the host erythrocyte cell membrane undergoes major remodelling in structure, composition and function [2]. The intra-erythrocytic parasites import nutrients for their development and export proteins and lipids into the host cell cytoplasm. This transportation occurs through New Permeability Pathways (NPPs), which selectively increases the permeability of the cell membrane of parasitized red blood cells (pRBCs) to a wide range of low molecular weight solutes [3]. An interconnected network of tubovesicular membranes (TVMs) is postulated to be responsible for the import of small molecules, whereas secretory cleft and lipid rafts may play a significant role in macromolecular transport in pRBCs [4]. Certain macromolecules like dextran, Protein A and IgG2 antibody are known to have direct access to the parasite through the “parasitophorous

duct,” a tubular membranous structure that extends between the parasitophorous vacuolar membrane and the erythrocytic membrane [5-7]. These changes are of interest for antimalarial chemotherapy, as possible routes for targeting parasitocidal drugs into pRBCs.

Nanocarrier-based systems are providing new and powerful opportunities for targeting malaria-infected erythrocytes for the treatment of the disease [8, 9]. The overall goal for effective antimalarial therapy is the achievement of high intra-cellular drug concentrations in pRBCs. This would require the drug to cross multiple membrane barriers to access the intra-parasitic targets, including the host erythrocyte membrane (HEM), the parasitophorous vacuolar membrane, the parasite plasma membrane and the food vacuolar membrane or endoplasmic reticulum membrane [10].

Human serum albumin (HSA) is a non-toxic, non-immunogenic, biocompatible and biodegradable protein and has been widely used to design nanoparticles for drug delivery, and includes the commercially available nanoparticle albumin-bound (nab) paclitaxel, Abraxane™ [11]. In addition, HSA, an endogenous transport protein with multiple drug binding sites can act as a versatile drug carrier and offer various possibilities of surface modification by appending ligands to modify pharmacokinetics, enhance stability, prolong circulation half-life, alter drug release or act as a targeting agent [12,13]. Notably high specificity and affinity interaction of native serum albumin with the parasitized erythrocytes have been reported [14]. Significantly, biotin-labelled and radio-iodinated HSA when added *in vitro* to malaria parasite cultures exhibited uptake, access to the parasite membrane through a membrane network and degradation in the parasite [15]. We took advantage of these features to use HSA as a nano-carrier for targeting anti-malarial drugs to pRBCs. The use of HSA to prepare nanoparticles for antimalarial drugs is an adept concept for selective targeting to pRBCs.

Artemether (ATM), a fast acting blood schizonticide is used as the current first-line therapy for severe multi-drug resistant malaria [16]. However, a very short half-life and poor aqueous solubility limits the clinical efficacy of this drug [17]. Currently, an oil-based

injectable formulation for intramuscular administration is available commercially. However, its use is limited due to its non-defined and erratic absorption. A suitable vehicle for intravenous delivery of ATM is urgently needed, especially for treating severe and cerebral malaria. HSA binds strongly to artemisinin and its derivatives through thiol and amino groups [18], paving the path to the development of artemether-loaded HSA-based nanoparticles which will open up opportunity for intravenous administration of artemether.

The aim of the present research was to develop and characterize HSA-based artemether nanoparticles for parenteral delivery and investigate their antimalarial efficacy and selective targeting to pRBCs. These nanoparticles were fabricated systematically using Quality-by-Design (QbD) approach. The nanoparticles were characterized for morphology, particle size, polydispersity index (PI), zeta potential, differential scanning calorimetry (DSC), X-ray diffraction (XRD) and Fourier transform infrared spectroscopy (FTIR) analysis. Their antimalarial efficacy was evaluated *in vitro* and *in vivo* using *Plasmodium falciparum* and *Plasmodium berghei* species, respectively. Pharmacokinetic studies after single intravenous injection were carried out in parasitized mice model to determine intra-cellular drug concentration in the RBCs. Confocal microscopy imaging was used to examine the entry of these nanoparticles selectively in pRBC in preference to non-infected RBCs. To best of our knowledge this is the first report of selective targeting of pRBCs using HSA based nanoparticles.

2. Experimental

2.1 Materials

Artemether was obtained as a gift sample from V. S. Internationals. HSA (Alburel) was purchased from Lifeline Pharmaceuticals, India. Absolute ethanol and polysorbate 80 were purchased from S. D. Fine chemicals Ltd. India. Trehalose was gift sample from Signet Chemicals, India. SYBR Green, hypoxanthine, gentamycin, formaldehyde solution, albumin bovine serum fraction V and 4' 6-diamino-2-phenylindole were procured from Sigma Aldrich, UK. Dextrose anhydrous, was sourced from Fisher Scientific, UK and Hepes medium was from Gibco, Life Technologies, UK. All solvents and chemicals used were of analytical grade.

2.2 *In vitro* culture of *Plasmodium*

Plasmodium falciparum parasites (strain 3D7 and K1) were grown in O+ve human RBCs in RPMI 1640 [+] L-glutamine, [+] Hepes medium supplemented with 5 mg/L albumin bovine serum fraction V, 50 mg/L hypoxanthine, 5 ml/L of 40% glucose and 50 mg/L of gentamycin (in PBS) in accordance with Read and Hyde [19]. Continuous culture of parasites at 5% haematocrit was carried out in 25 or 12.5 cm² flasks, in final culture volumes of 10 ml and 5 ml respectively with sub culturing at 48 and 72h intervals. Synchronization of parasite stages was achieved by adding sorbitol solution (5% w/v in distilled water filtered through a 0.22 µm filter) to the parasite pellet with a 5 min incubation. The culture was centrifuged at 3,000 rpm for 5 minutes and the supernatant discarded. The pellet was washed three times in complete RPMI prior to re-suspension at the appropriate haematocrit. Preliminary estimation of parasitaemia was carried out using Giemsa-stained thin blood smears. Culture flasks were gassed with a 5% CO₂, 5% O₂, 90% N₂ air mixture (BOC Limited, UK) and incubated at 37°C (Leec 190 CO₂, Leec Limited, UK).

2.3 *In vivo* culture of *Plasmodium*

The *P. berghei* ANKA strain was used for *in vivo* evaluation of antimalarial activity. The strain is well characterised with high mortality in mice. The parasites kept in liquid nitrogen were thawed (at 37 °C) and parasitic culture was maintained in live mice through serial blood transfusion in fresh animals every 4 days. Animal experiments were carried out as per the protocols (CUSCP/IAEC/43/2012 and CUSCP/IAEC/31/2013) approved by Institutional Animal Ethics Committee of SNDT Women's University, Mumbai. Research was conducted in accordance with guidelines on animal use and care and followed internationally accepted principles for laboratory animal use and care. Swiss albino mice of either sex aged 9-10 weeks and weighing 22-27g were used for the experiment. The animals were quarantined at a temperature of 22±3⁰ C and 65% relative humidity and were fed a standard pelleted diet and provided with clean drinking water, throughout the experiment.

2.4 Development of artemether-loaded HSA nanoparticles

Artemether-loaded HSA nanoparticles (AAN) were prepared using the desolvation technique [20-22] followed by high-pressure homogenization. Briefly, HSA (Alburel) was diluted with water to obtain the desired concentration (2% w/v) and pH was maintained at neutral. The drug was dissolved in a mixture of ethanol (40% v/v) and polysorbate 80 (3%w/v), which was slowly injected in the protein solution. The dispersion was cross-linked by heating and homogenised in a high-pressure homogeniser (Niro Saovi Panda Plus). The nanoparticles thus obtained were lyophilised in presence of trehalose as cryoprotectant in a freeze dryer (Martin Christ Epsilon 2-4LSC). A 48 hour cycle was divided into three phases of 6, 18 and 24 hours for the stages of freezing, main drying and final drying, respectively (Table S1). Blank nanoparticles (BAN) were prepared using exactly the same protocol without addition of any drug. Rhodamine B (2.5µg) was covalently bound to AAN (1 ml) using 1-ethyl-3-(3-dimethylaminopropyl) carbodiimide hydrochloride (EDC)/N-hydroxysulfo-succinimide (sulfo-NHS) reaction with incubation at room temperature for 3 h to prepare rhodamine labelled nanoparticles [23, 24]. The labelled nanoparticles were subjected to dialysis against deionized water to remove any excess dye. Briefly 1 ml Rhodamine B tagged nanoparticles were put in dialysis membrane (3K MWCO) bag and suspended in beaker filled with 1000ml deionised water with continuous magnetic stirring for 1 h.

Systematic optimization of the formulation was carried out using the QbD approach [25]. The Ishikawa diagram was used to determine the critical quality attributes (CQA) of the entire process (Fig 1). The method was optimised for materials, process and environment related factors (Table 1) to correct the CQAs during the development. Apart from conventional optimisation with one factor at a time, two 3² factorial designs (9 runs each) were applied to optimise the material related parameters. Design I investigated the effect of HSA (at three levels; 1,2 and 3% w/v) and solvent concentration (at three levels; 20,30 and 40% v/v) and design II investigated the effect of HSA (at three levels; 1,2 and 3% w/v) and surfactant concentration (at three levels; 3, 5 and 7% w/v) on the particle size of the nanoparticles (Table 2). Design Expert 8.0 was used to build response surface curves. Process related parameters, i.e., homogenisation pressure and number of homogenisation cycles were optimised by varying the homogenisation pressure from 200 to 1400 bars with 1 to 20

homogenisation cycles (20 runs Table S2). Environment related factors like pH, type and concentration of cryoprotectant were also optimised.

2.5 Fluorescence spectroscopy for determination of binding of artemether to HSA

Fluorescence spectroscopy helps in understanding the residues that are involved in the drug-carrier interaction. Fluorescence spectra of HSA alone and in the presence of different concentrations of artemether were taken at excitation wavelength (λ_{ex}) of 280nm and emission wavelength (λ_{em}) from 290 to 400nm on Perkin Elmer LS55 fluorescence spectrometer. Fluorescence spectra of blank HSA nanoparticles (BAN) and AAN were also recorded. The fluorescence quenching data was analysed according to the Stern–Volmer equation [26, 27]

$$F_0/F = 1 + K_{sv} [Q]$$

F_0 and F denote fluorescence intensities in the absence and presence of quenchers respectively. K_{sv} is the Stern-Volmer constant and $[Q]$, the quencher concentration.

2.6 Characterisation of artemether-loaded HSA nanoparticles

2.6.1 Particle size and Polydispersity index

AAN was characterised for mean particle size and PI using photon correlation spectroscopy (PCS) technique employing N5 Beckman particle size analyser Inc., USA. All measurements were carried out at a fixed angle of 90° at 20°C using double distilled water as dispersant. The averaged values three measurements are presented.

2.6.2 Morphology

The microstructures of AAN particles were observed using transmission electron microscope (TEM) (Philips CM 200). Initially, sample diluted with double-distilled water was deposited on film-coated copper grids and allowed to dry overnight at room temperature. The dried samples were visualized under TEM. Size and morphology of lyophilised nanoparticles were examined using a field emission scanning electron microscope (SEM) (Model JEOL JSM-7600F). AAN particles were first coated in gold to minimize the effect of heat during high power magnification.

2.6.3 Differential Scanning Calorimetry (DSC)

DSC measurements on ATM, HSA and AAN were performed using a Q200 TA instrument (New Castle, Delaware, USA). The heating runs were performed from 30°C to 200°C at 10.0°C/min. An empty aluminium pan was used as a reference.

2.6.4 Fourier Transform Infrared (FT-IR) spectroscopy

The interaction between the drug and carrier and the encapsulation of drug was evaluated using FT-IR spectroscopy using JASCO FTIR 5300 Spectrometer with TGS detector (MD, USA) over the scanning wavelength range of 4000 – 400 cm⁻¹. Potassium bromide disc method was employed to obtain FT-IR spectrums of AAN as well as the individual components.

2.6.5 X-ray Diffraction (XRD) Studies

XRD studies of ATM and AAN were performed using Philips Expertpro MPD diffractometer (PAN analytical Inc. Germany) with resolution of 0.001 Å⁰. The samples were radiated using a Cu target ($\lambda = 1.54056 \text{ \AA}$) and scanning angles ranged from 7⁰ to 70⁰ of 2 θ .

2.6.6 Determination of entrapment efficiency

Entrapment efficiency was determined by separating the nanoparticles from aqueous dispersion by ultracentrifugation (30000g at 4⁰ C for 1h) and the amount of free drug in the clear supernatant was analysed by UV-spectroscopy (UV 2450, Shimadzu, Japan) [16]. The encapsulation efficiency was calculated by using the following equation:

$$\frac{W - w}{W} \times 100$$

where W = amount of ATM initially added and w = amount of ATM present in the supernatant

2.6.7 In vitro Drug release

In vitro drug release study was performed in modified USP type II apparatus (Electrolab, India Pvt Ltd.). 3ml of AAN dispersion or reconstituted lyophilised AAN nanoparticles were enclosed within cellulose acetate dialysis bag (3K MWCO) and placed in 200 ml of

phosphate buffer saline (pH 7.4): ethanol (50:50) as dissolution medium to maintain sink conditions. The medium was continuously stirred at 100 rpm and maintained at $37\pm 5^{\circ}\text{C}$. 5ml aliquots were withdrawn at predetermined time points (0.5, 1, 2, 4, 6, 8 and 24 h) and were replaced with the same volume of dissolution media. The concentration of drug released was analysed by UV Spectroscopy (UV 2450, Shimadzu, Japan) [17].

2.7 *In vitro* erythrocyte toxicity study

Infection with *P. falciparum* result in erythrocyte rupture during its intra-erythrocytic life cycle causing haemolysis leading to anaemia in severe conditions [28]. For an antimalarial drug delivery system, it is important to have action targeted specifically on pRBCs with no harm to the uninfected erythrocytes. The *in vitro* erythrocyte toxicity study determines the toxicity potential of the system on the uninfected erythrocytes on intravenous administration.

The test was performed using varying dilutions of AAN in normal saline (1X, 10X and 100X). Polysorbate 80 (3% w/v) and Triton X 100 (2% w/v) in normal saline were used as reference and positive control respectively. 100 μl of the prepared human RBCs were incubated with 900 μl of the test solutions for 30 minutes. The reaction was stopped by addition of glutaraldehyde. The tubes were centrifuged to separate the debris and the supernatant was analysed for the haemolytic activity by measuring the absorbance at 540nm by UV spectrophotometry (UV 2450, Shimadzu, Japan). The percent haemolysis was calculated by the formula:

$$\% \text{ Haemolysis} = \frac{\text{Absorbance of sample} - \text{absorbance of control}}{\text{Absorbance of Triton X 100} - \text{absorbance of control}} \times 100$$

2.8 *In vitro* susceptibility assay

Antimalarial drugs are maximally active on the mature trophozoite stage of parasite development. *In vitro* susceptibility has been correlated with the initial stage of the parasite, with isolates predominantly at the trophozoite stage having a twofold increase in IC50s compared to those of parasites predominantly at the ring stage [29,30]. The *in vitro* antimalarial efficacy was therefore assessed using synchronised trophozoite stage cultures of *P. falciparum* (K1) parasite strains reported previously [31]. 5 mM stock solution of

artemether (MW 298.38) in DMSO (ATM) was used to produce a dilution series for the dose response curve. AAN and BAN nanoparticles were reconstituted aseptically with sterile-filtered double-distilled water. 0.2ml of the *P. falciparum* culture (5% haematocrit and 0.5% parasitaemia) was seeded in a 24-well plate and formulations and drug solution added along with complete media. The drug dose range was tested at 0.78, 1.56, 3.13, 6.25, 12.5 and 25 nM concentrations. The plates were incubated for 48h at 37°C and parasitaemia was determined by SYBR green-based flow cytometry methods as described previously. Briefly, triplicate drug/nanoparticle treated parasite cultures (100µl each) are transferred to Eppendorf tubes and washed in 1 ml PBS, and centrifuged at 1400 rpm for 90 secs. The pellet is resuspended in 1 ml 2.5 x SYBR Green 1 and incubated in the dark for 20 mins at room temperature. Samples were centrifuged as described and re-suspended in 250 µl of a fixative solution of 0.4% formaldehyde solution and incubated at 4°C for 15 mins. The pellets were washed three times in PBS and suspended in 1 ml of PBS for flow cytometric analysis on a BD FACSVerse flow cytometer (USA). 50,000 events were recorded for each sample using the FITC channel and fluorescent intensity recorded. Percent inhibition was calculated against the drug-free control.

2.9 Determination of cellular uptake of nanoparticles by confocal microscopy

Synchronized ring stage parasite cultures (200 µl) were incubated with Rhodamine B-labelled AAN (25 µl) along with complete media (1ml) in a 24-well cell culture plate, at 37°C. The cellular uptake was observed at pre-determined time points of 15 min, 1 h and 24 h. The cells were washed with RPMI-1640 culture medium and stained with parasite nucleic acid stain 4',6-diamino-2-phenylindole (DAPI) for 20 mins to distinguish pRBCs from normal RBCs. At each of the time points, a small sample (5 µl) was removed from a stock culture of pRBC and wet mounted on a clean glass slide with a coverslip placed on it for examination. The cellular uptake was observed at a magnification of 100X using confocal laser scanning microscope (ZEISS LSM 510 META, Germany) at an excitation wavelength of 540 nm and an emission maximum of 625 nm. As a positive control, pRBCs were stained with DAPI to distinguish them from uninfected RBCs and observed at excitation maximum of 358 nm and emission maximum of 461nm.

2.10 *In vivo* antimalarial efficacy in *P. berghei* infected mice

The lethal ANKA strain of *P. berghei* was used for the experiments [32]. Mice of either sex (average weight 25g) were infected by intraperitoneal inoculation of the parasite obtained from the donor mouse blood diluted with citrate phosphate dextrose containing approximately 5×10^7 -infected RBCs/ml. The mice were randomly divided into various groups (n = 5) (Table 4). Post-infection, the animals were treated with AAN aseptically reconstituted using sterile saline at two dose levels 0.624mg/day and 0.312 mg/day (equivalent to 100 and 50% of therapeutic dose of artemether) for four consecutive days. In lack of marketed intravenous artemether injection, artesunate (ARS), which has been previously employed for comparison in developmental antimalarial intravenous products [33,34], was used as reference. Larinate, marketed intravenous ARS injection, was reconstituted using the provided diluent under aseptic conditions and injected at same dose levels as AAN. Blank nanoparticles (BAN) were administered in volume equivalent to AAN containing 0.624mg of drug in AAN. On day 0, 1, 5, 7, 10, 14 and 21, day thin blood smears were prepared by collecting a drop of blood from the tail vein. The blood smears were air-dried, fixed in methanol and stained with Giemsa stain. The smears were then washed, air-dried and observed under the microscope using an oil immersion lens and parasitaemia was assessed. The study parameters involved (i) number of surviving animals from each group on day 30 (ii) mean percent parasitaemia over time (in days) for all groups. Data was expressed as mean \pm S.D. and assessed by unpaired t-test using the Graph-pad InStat Demo version. A difference of $P < 0.05$ was considered as significant.

2.11 Pharmacokinetics in *P. berghei* infected mice

The parasitized animals were divided into three groups of six mice per group. When animals reached parasitaemia of 50-60% the first group was administered AAN as single dose (35 mg/kg equivalent amount of artemether) intravenous injection. Artemether free drug being insoluble in water its solution was prepared by dissolving it in non clinical hydroalcoholic vehicle (ATM) [35] and administered intravenously to the second group while third group acted as control. At stipulated time interval of 10min, 30min, 1, 2, 4, 8, 10, and 24h, the

animals were exposed to inhalation of anaesthetic ether and blood samples were withdrawn using retro-orbital puncture. The blood samples were centrifuged at 2000 rpm for 10 min and the supernatant plasma and RBCs were collected in two separate clean Eppendorf tubes. To the 200 μ l plasma sample, 100 μ l of internal standard (artemisinin) and 700 μ l of acetonitrile was added and the contents of the tube were vortexed and then centrifuged at 2000 rpm for 10 min using mini centrifuge (Hoefer, USA) [36]. Similarly for extraction from RBCs, to 200 μ l of RBC sample, 100 μ l of internal standard, 20 μ l ammonium chloride buffer (for haemolysis of RBCs) and 680 μ l of acetonitrile were added. The mixture was vortexed and centrifuged at 2000 rpm for 10 min (Hoefer mini centrifuge). The upper organic layer from each of the extractions was filtered and analysed using HPLC (Agilent 1200 series, Singapore) equipped with C18 column (Princeton SPHER ODS, 250 x4.0 mm; 5 μ ,) with PDA detector. Acetonitrile: water (75:25 v/v) was used as mobile phase at flow rate of 0.7 ml/min. and detection wavelength was set at 210nm [37]. Each solution was injected in triplicate and mean peak areas were recorded for quantification for the drug.

3. Results

3.1 Development of artemether-loaded HSA nanoparticles

Basic methodology and all the essential material and process parameters required for development of nanoparticles were derived in reference to the Ishikawa Diagram (Fig 1). Risk identification and risk analysis of material, process and environment variables (Table 1) provided parameters for control strategy for the CQAs [25]. Optimization of the formulation was performed to reduce the risk of the CQAs to obtain a robust and reproducible formulation.

Concentration of HSA and Drug: HSA ratio was optimised based on the particle size and entrapment efficiency of the drug. Increasing the HSA concentration resulted in increase in particle size (Fig 2a) hence, 2% w/v concentration was found to be optimum showing negligible drug precipitation and lower particle size [20]. Incorporating ATM at drug: HSA ratio of 1:5 resulted in precipitation of drug while 1:20 ratio led to increase in particle size without added advantage in loading efficiency thus drug: HSA ratio of 1: 10 was found optimum (Table 3). ATM being highly water insoluble drug, incorporation of polysorbate 80

stabilised the nanoparticles with positive effect on drug entrapment (Fig 2c) [38, 39]. Concentrations of HSA, ethanol and polysorbate 80 were further optimized using two 3^2 full factorial designs. The P-values of 0.0009 and 0.0274 indicated that the models were significant. Reducing the HSA concentration and increase in ethanol concentration resulted in smaller particle size (Fig 2d) [40]. The blue region in the response surface curve (Fig 2e) shows the area of lowest particle size, which could be achieved at the optimum HSA and surfactant concentration levels

Increasing the pH (>7) of the HSA solution prior to desolvation decreased the particle size of the nanoparticles (Fig 2b), due to increased repulsion between the molecules preventing their aggregation. This observation is in good agreement with previously published literature [20, 41]. However ATM precipitated at higher pH, therefore it was important to maintain the pH of the HSA solution at 7 throughout the process. This could be explained by different HSA conformations at different pH values. The standard HSA conformation “N” is present at neutral pH. A change to the “B” conformation occurs above pH 8 which might have lower affinity to ATM [42]. Similar observations have been earlier reported [43].

High-pressure homogenization was used to prepare HSA nanoparticles [44]. Effect of homogenization pressure and number of homogenisation cycles were seen to play an important role in determination of particle size. It was found that lower homogenisation pressures were sufficient to get the desired particle size (<100nm) and PI. Higher pressures led to increase in particle size [Supplementary data Table S2]. Though earlier reports have shown reduction in particle size with increase in homogenisation pressure for HSA nanoparticles, a minimum particle size of 222.2 nm could only be achieved at high homogenisation pressures [45].

3.2 Freeze drying of nanoparticles

AAN was freeze-dried to get a free flowing stable product. Freeze-drying of AAN without cryoprotectant and with mannitol and lactose as cryoprotectants resulted in increased particles size and PI (Fig 3) [46]. Trehalose at 3% w/v concentration was found useful as cryoprotectant for lyophilisation of nanoparticles with neither a significant change in particle

size (3a) nor in polydispersity index (Fig 3b). Trehalose is known to preserve the HSA nanoparticle during freeze-drying as it forms amorphous glass, which is reported to interact with amorphous protein in the freeze-dried cake [47].

3.3 Fluorescence spectroscopy for determination of binding of artemether to HSA

Fluorescence quenching of the single tryptophan residue in HSA was used to measure drug-binding affinity [48]. When HSA is excited at 280 nm, fluorescence intensity around 350 nm reflects changes of the microenvironment of tryptophan residue. Addition of ATM showed dynamic quenching of the fluorescence of HSA (Fig S4) and followed Stern Volume equation with K_{sv} of $1.755 \times 10^4 \text{ L.mol}^{-1}$ [26]. A strong decrease in the fluorescence intensity in the spectra of AAN nanoparticles (650a.u) was observed in comparison with the blank nanoparticles (900a.u) (Fig. 4) suggesting interaction of ATM and HSA. The quenching process also signifies the tertiary structural changes in HSA demonstrating binding of drug with HSA in the nanoparticulate formulation [49].

3.4 Characterization of the nanoparticles

Mean particle size of AAN was found to be 66.1nm (PI 0.090) by PCS and was in confirmation to that obtained from TEM and SEM (Fig 5) of the freeze-dried product (Fig 5d) with zeta potential from -14.9 mV. TEM and SEM images both confirmed almost spherical morphology of AAN.

DSC thermogram of ATM and HSA exhibited endothermic peaks at 85.73°C and 126.97°C respectively. AAN showed a shift in the peak to 160.45°C because of drug-albumin binding and formation of nanoparticles [20], although a small peak near the endothermic peak of the drug may be indicative of small amount of ATM present on the surface of HSA matrix (Supplementary data Fig S1).

XRD pattern of ATM shows the presence of sharp peaks indicating the crystalline nature of the drug. The XRD of HSA exhibited a broad reflection with no distinct peaks revealing the amorphous structure of HSA. Absence of sharp peaks of artemether and broad humps in

the AAN graph indicated that the drug was successfully incorporated into the HSA nanoparticles and was present primarily in an amorphous form within the nanoparticles (Supplementary data Fig S2) [50]. However, some sporadic weak peaks in AAN might indicate that ATM might not be not fully shielded by protein side chains and small amounts present on the surface. This is in accordance with our DSC results and consistent with a previous study [51].

All the characteristic peaks of HSA observed in the FTIR were retained in the AAN indicating no chemical modification in the structure of the protein. The spectra of AAN revealed the characteristic peaks of ATM with almost negligible shifts from which it may be deduced that artemether is entrapped within the HSA matrix and that the chemical structure of artemether does not change after encapsulation (supplementary data Fig S 3). Similar FTIR spectroscopy results have been demonstrated for encapsulation of bioactive molecules into albumin nanoparticles [40,52].

In vitro release curves (Fig 5) of ATM from AAN showed an initial burst effect followed by slow release. This could be because of the different ways in which the drug is loaded in the nanoparticles: adsorption and entrapment [53]. Lyophilisation of nanoparticles did not have any effect on the drug release and was similar to that obtained from nanoparticles prior to lyophilisation.

3.5 *In vitro* erythrocyte toxicity study

ATM being practically insoluble, required polysorbate 80, a non-ionic surfactant to be incorporated in the formulation to improve its solubility and drug entrapment. Surfactants may cause damage to cell membranes of erythrocytes due to increases in membrane permeability [54] and therefore an *in vitro* erythrocyte toxicity test was carried out to evaluate biocompatibility of the nanoparticles [55] Triton-X-100 (positive control) showed 100% haemolysis of erythrocytes throughout the incubation period. Though polysorbate 80 solution (3% w/v) exhibited haemolysis of 75.89% after 30 min incubation, AAN containing 3% w/v polysorbate 80 showed an erythrocyte haemolysis rate of only 9.92% (Fig. 6), demonstrating

its safety. An earlier report by Joshi *et. al.*, has shown very low erythrocyte haemolysis of NLC even at very high concentrations of surfactant [32]. This might be due to micelle formation of the surfactant at the nanoparticle and water interface, resulting in solubilisation of the drug and stabilisation of the entire system. Previous experiments have shown that a polysorbate 80 coating on the surface of HSA nanoparticles possess reduced toxicities and improved pharmacokinetic parameters of doxorubicin [56]. Clinically, upon administration, drugs injected intravenously are immediately diluted to a very large extent due to constant blood circulation and sink conditions provided by the body. To mimic *in vivo* conditions, diluted formulations were also tested for their haemolytic potential. AAN showed a haemolysis of 6.24% when diluted 10 times and 6.12% when diluted 100 times at the end of 30 minutes (Fig 5).

3.6 *In vitro* susceptibility assay

Treatment of *P. falciparum* cultures with ATM and AAN demonstrated a dose-dependent anti-parasitic effect while BAN, the HSA nanoparticle without any drug, failed to show any effect (Fig. 7) [57]. AAN displayed optimal enhancement of anti-malarial activity in a concentration range of 3.13 to 12.5 nM. At concentrations that were too low to effectively kill the parasite, insignificant differences were observed in the efficacy of drug solution and particles. Similarly, when drug concentrations were high enough to overcome rate-limiting diffusion and provide intracellular parasitocidal concentrations, the efficacy of particles was no different from that of the drug in solution. However, in a window of intermediate concentrations, the advantages of drug targeting using nanoparticles were unambiguously apparent. Maximum difference in inhibition of parasitaemia was evident at 6.25 nM drug concentrations of ATM demonstrating significantly ($p < 0.001$) higher antimalarial activity with AAN as compared drug solution. IC_{50} values of AAN and ATM solution were 5.4 nM and 12.08 nM respectively, evidencing improvement in efficacy at comparative IC_{50} dosages .

3.7 Determination of cellular uptake of nanoparticles by confocal microscopy imaging

Nanoparticles attached on the surface of erythrocytes possess extended circulation time in the body [58]. Nano-sized particles (≤ 200 nm) have been shown to enter the RBC however;

the translocation mechanism is not clear and remains controversial [59] Therefore, study was carried out to analyse actual entry of the nanoparticles into the plasmodium-infected erythrocytes.

DAPI staining helped in differentiating between parasitized and non-parasitized RBC in the co-cultures since DNA of the parasite is stained blue which is only present in the pRBC (Fig.8) [60]. Rhodamine-labelled AAN incubated with Plasmodium-infected RBCs showed time-dependent uptake selectively by pRBCs as evident by co-located red fluorescence in DAPI stained cells. (Fig 8). The uptake starting at as early as 5 minutes of incubation and the fluorescence was found to persist till the rupture of pRBC. The uptake of nanoparticles was confirmed by Z-stacking of the confocal images which showed presence of fluorescence due AAN in various sections of the pRBCs (Fig S5). All the confocal images confirmed that nanoparticles do not penetrate the normal non-infected RBCs as was evident by absence of red fluorescence of rhodamine-labelled nanoparticles in these cells (Fig 8).

3.8 *In vivo* antimalarial efficacy in *P. berghei* infected mice

Nanostructured lipid carrier [32] and lipid nanoparticles [61] of artemether have shown improved antimalarial activity in *P. berghei* model. Peter's four-day suppressive test was performed on AAN at two dose levels viz, 100 and 50% of therapeutic dose of the drug using *P. berghei*-infected Swiss albino mice. Due to absence of any intravenous injection for artemether, Larinate (artesunate injection), which is administered as intravenous injection was used as the reference.

The control group showed highest parasitemia at all-time intervals with maximum of 72.13% on day 10 with all mice found to be dead after 10th day. As compared to the control group, all the other groups showed reduction in the parasitemia during the course of study ($p < 0.001$), analysed by one-way ANOVA followed by Tukey's multiple comparison test. Marketed formulation showed reduction in parasitemia (23.46%, day 21) as compared to control at 100% dose level, however the reduction in parasitaemia was much less (46.34%, day 21) and the survival rate of animals was reduced to half (Table 4) when the dose was

reduced to 50%. Parasitaemia with AAN was found to be 13.21% at 100% dose and 13.71% at 50% dose level at the end of 21st day of the experiment. AAN showed significantly less ($p < 0.001$) parasitaemia as compared to marketed intravenous injection of artesunate at both the dose levels (Fig 9). Blank nanoparticles showed reduction in the parasitaemia (30.48%) on 21st day as compared to the control. Previously Blank NLC (placebo vehicle) has also shown reduction in the parasitaemia [32]. The reason for the activity is not known since none of the excipients is known to have any antimalarial activity. The surfactant used in the formula might be responsible for the parasitic cell haemolysis due to increased permeability of the parasitized cell, which might have resulted in the activity. Interestingly albumin has been reported to reduce mortality when given as adjunct therapy in children with severe malaria (62).

3.9 Pharmacokinetics and erythrocyte drug concentration in *P. berghei*-infected mice

AAN showed higher drug concentrations in the erythrocytes and deliver their payload to the target cell more efficiently than the molecular drug solution. AAN showed two times higher peak drug concentration in the RBCs as compared to ATM solution (Fig 10a). This is consistent with the results obtained in *in-vitro P. falciparum* studies, which showed increased intracellular uptake by pRBCs and higher inhibition of parasitaemia by AAN. This is also reflected by higher AUC_0^{24} ($p < 0.05$) in the RBCs after administration of AAN ($1017.5 \pm 107 \mu\text{g}\cdot\text{min}/\text{ml}$) as compared to ATM solution ($554.5 \pm 68 \mu\text{g}\cdot\text{min}/\text{ml}$). After intravenous administration, AAN and ATM showed high initial plasma concentrations followed by constant decline with very low concentrations remaining at the end of 10h and no drug in plasma at 24h. AAN revealed lower drug levels in plasma as compared to ATM probably because of partitioning more into RBCs (Fig. 10 b)

4. Discussion

Clinical management of severe and cerebral malaria remains a challenge with varying degrees of success even with parenteral administration of potent anti-malarial agents. Drug delivery strategies that can target the antimalarial drugs selectively to the pRBCs can potentially reduce drug exposure to non-target sites, delivering high drug concentrations to the infected cells and reducing the risk of drug resistance. In this study, we show HSA

nanoparticles to be selectively taken up by pRBCs leading to higher local drug concentrations and improved antimalarial efficacy.

Robust HSA nanoparticles were developed using the QbD approach. An industrially feasible and scalable process of high-pressure homogenisation was used to fabricate the nanoparticles [44]. ATM being water insoluble is presently available as an oily intramuscular injection. HSA showed strong binding to artemether (Fig 4f) and with resultant physical linkages facilitated nanoparticle formation. Addition of polysorbate 80 (3% w/v) stabilised the nanoparticles and prevented drug precipitation, leading to formulation of an aqueous injection of ATM with high drug loading [39]. Addition of polysorbate 80 had no discernible adverse effect on the cell membrane of erythrocytes, as demonstrated by low haemolytic activity (<10%), which was further reduced on dilution (Fig 5). The nanoparticles can be considered safe for intravenous administration.

It is important to control the size of the prepared nanoparticles because smaller sized particles improve the bioavailability, with increased ability to enter cells. It has been reported that only NLCs <400 nm diameter were taken up by pRBCs. [63]. In another study, it was determined that fluorescent latex beads >172 nm did not access intracellular parasites [7]. In our study we aimed to prepare nanoparticles having particle sizes less than 100 nm. HSA concentration critically affected the particle size and drug entrapment. While higher HSA concentrations led to increase in particle size, lower concentrations decreased the drug entrapment. The average size of the particles also decreased with increase in the percentage of added ethanol [40, 64]. In this context, the optimised nanoparticles with Drug:HSA ratio of 1:10 at 40% ethanol concentration as desolvating agent produced the smallest nanoparticles with highest drug loading (77.6%). Low homogenisation pressure 200 bar (10 cycles) followed by 5 cycles at 400 bar was sufficient to yield mean particle size of 66.1 nm and PI of 0.090. Higher homogenisation pressures resulted in a larger particle size. This can be explained as follows; the additional energy input resulted in higher kinetic energy of the particles with subsequent coalescence. Once the maximum dispersitivity has been reached additional energy put into the system cannot be used for further dispersion of nanoparticles. The energy put in can only accelerate the velocity of the particles, giving them adequate

kinetic energy to overcome the stabilization resulting in aggregation and increase in mean size [65].

Since ATM is known to be moisture sensitive, drug freeze-drying was investigated to retain the stability of AAN. Freezing often induces many destabilizing stresses for nanoparticles. Formation of ice crystals that can mechanically destabilize nanoparticles and increased interaction due to enhanced nanoparticle concentration leading to aggregation or fusion are some of the phenomena observed during freeze drying [66]. Trehalose as an additive seems to provide sufficient protection from lyophilization of HSA protein, contributing to maintaining stability in the solid state [67]. Trehalose containing formulations were superior to mannitol and lactose, exhibiting minimal increases in nanoparticle size and PI following the freeze-drying procedure (Fig 3a,3b) [68].

The release of drug from AAN was characterised by a biphasic release pattern with an initial burst release ($t_{50\%}$ - 4.6h) followed by sustained drug release ($t_{90\%}$ - 25.3h) (Fig 5e). The initial fast release is attributed to the weakly interacted drug associated with surface of the nanoparticles. Subsequently, the entrapped ATM released from the core of the nanoparticles in a sustained manner due to the diffusion of drug across the albumin matrix, would provide the possibility of continual drug effect. A similar phenomenon was observed previously in albumin nanoparticles [69-71]. However the association of the drug with the carrier material in competition with other carriers such as plasma proteins, lipids, and cell membranes plays an important role for the performance *in vivo* [72].

In vitro susceptibility assays in *P. falciparum* demonstrated significantly ($p < 0.001$) higher antimalarial activity with AAN as compared drug-only control as demonstrated by the lower IC_{50} values of AAN. This was confirmed by *in vivo* studies where AAN showed high antimalarial activity even at 50% dose in *P. berghei* infected mice. While the chemosuppression was reduced from 76.54% to 53.66% when free ARS dose was reduced to 50%, chemosuppression did not change significantly ($p > 0.05$) showing equal activity (86.79 and 86.29%) at 100 and 50% doses respectively with AAN.

Confocal images clearly discriminated the selective uptake of Rhodamine-labelled AAN particles by pRBCs and not by normal RBCs. The amount of nanoparticles entering the pRBC was found to increase with time. It is a well-known fact that, mature erythrocytes do not display endocytosis and no pathways are evident for up taking macromolecules by these cells [73,74]. But contrary to this, uptake of ferritin claiming that *Plasmodium*-infected red cells are capable of endocytosis have been reported [75]. Many changes occur in the host cell membrane during intracellular malarial parasite development with extensive degradation of spectrin, allowing endocytosis in pRBCs [76,77]. Parasites are capable of enhancing the permeability of cell membranes in the host through NPP [78,] and TVM [79] allowing nutrients access to the parasite. This increased permeability differs from the native transport systems of the normal erythrocyte [80,81]. Membrane-impermeable macromolecules in the external medium have been shown to bypass the host cell cytosol to reach intracellular parasites [82,83]. Though internalisation mechanisms remain to be elucidated, it is speculated that HSA nanoparticles would follow similar uptake pathways, as HSA which has been reported to have direct access through the parasitophorous duct [5,6,15] into the pRBCs as a nutritional requirement [15,84,85]. Pouvelle *et al.*, have demonstrated the presence of tubular prominences, which develop in the cytoplasm of the pRBC that link up with the host cell membrane to form a transient or stable duct, providing a means of direct access between the parasite and the external milieu [86]. An alternative concept of a 'metabolic window' that forms during the ring stage of asexual parasite maturation, provides 'contact sites' between the HEM and the PVM [87]. The altered membrane permeability coupled with capability for endocytosis could be key factors responsible for the entry of the nanoparticles selectively into the pRBCs [2, 5, 75, 80].

Previously, Hasan *et al.*, reported on the entry of stearylamine liposomes into the pRBC when observed using fluorescent microscopy [88]. Chloroquine liposomes loaded with quantum dots, covalently functionalized with oriented, specific half-antibodies against *P. falciparum* have been found to dock to pRBC plasma membranes and release their cargo into the cell [89]. More recently polymers poly(amidoamines) AGMA1 and ISA23 have exhibited preferential binding to and internalization into *P. falciparum* and *P. yoelii* infected RBCs [90]. However safety of these systems have not been definitively established. HSA

being endogenous, stable, biocompatible and already commercially exploited for other applications has a distinct advantage over these nanosystems and could be a safer, new tool for targeting drugs to *Plasmodium* infected cells. Improved activity and the associated reduction in parasitaemia with AAN, could be attributed to parasite clearing as a result of selective cellular uptake of nanoparticles by pRBCs as observed by confocal microscopy.

5. Conclusion

In conclusion, biodegradable artemether-loaded HSA-based nanoparticles were developed as an intravenous drug delivery system for the treatment of malaria. Robust formulation with reproducible particle size was successfully obtained employing the QbD approach. *In vitro* studies using *P. falciparum* showed a 50% reduction in IC₅₀ values of AAN when compared with drug only controls. AAN showed marked less parasitaemia as compared to marketed intravenous injection of artesunate and showed equivalent antimalarial activity at half the therapeutic dose. Uptake of nanoparticles by pRBCs was demonstrated by higher intracellular drug concentration in the erythrocytes as shown by the pharmacokinetic studies in the parasitized mice. Confocal imaging confirmed the selective entry of the nanoparticles into pRBCs, but not healthy uninfected RBCs. A follow-up quantitative fluorescence-assisted cell sorting analysis study is proposed as part of further work. Thus, HSA nanoparticles have shown significant potential to be used as a safe and effective drug delivery system for the treatment of malaria. As it permits intravenous administration and selective pRBC uptake, it can be a beneficial strategy in severe and cerebral malaria.

References

1. WHO, World Malaria Report (2014), <http://www.who.int/malaria/publications/world> accessed on 30th November 2015.
2. Elford TB, Cowan GM and Ferguson DJP. Parasite-regulated membrane transport processes and metabolic control in malaria-infected erythrocytes. *Biochem. J.* 308, 361-374 (1995).

3. Kirk K, Tilley L, Ginsburg H. Transport and Trafficking in the Malaria-infected Erythrocyte. *Parasitol. Today* 15, 355-357 (1999).
4. Haldar K, Samuel BU, Mohandas N, Harrison T, Hiller NL. Transport mechanisms in Plasmodium-infected erythrocytes: lipid rafts and a tubovesicular network. *Int. J. Parasitol.* 12, 1393-401 (2001).
5. Pouvelle P, Spiegel R, Hsiao L, et al. Direct access to serum macromolecules by intraerythrocytic malaria parasites. *Nature*, 353, 73–75 (1991).
6. Chairpan S, Przyborski JM. Protein transport across the parasitophorous vacuole of Plasmodium falciparum: into the great wide open. *Traffic* 9, 157-165 (2008).
7. Goodyer ID, Pouvelle B, Schneider TG, Trelka DP, Taraschi TF. Characterization of macromolecular transport pathways in malaria-infected erythrocytes. *Mol. Biochem. Parasitol.* 87, 13–28 (1997).
8. Aditya NP, Vathasal PG, Vierira V, Murthy RSR, Souto EB. Advances in nanomedicines for malaria treatment. *Adv. Colloid Inter. Sci.* 201-202, 1-17 (2013).
9. Singh KK. Nanomedicine in Malaria. In: *Patenting Nanomedicine: Legal Aspects. In Intellectual Property and Grant Opportunities.* Souto EB. (Ed.), Springer Link, 401-435 (2012).
10. Bannister LH, Hopkins JM, Fowler RE, Krishna S, Mitchell GH. A Brief Illustrated Guide to the Ultrastructure of P. falciparum Asexual Blood Stages. *Parasitol. Today* 16, 427-433 (2000).
11. Cortes J, Saura C. Nanoparticle albumin-bound (nabTM)-paclitaxel: improving efficacy and tolerability by targeted drug delivery in metastatic breast cancer *European Journal of Cancer Supplements* 8, 1–10 (2010).
12. Elzoghby A, Samy W, Elgindy N. Albumin-based nanoparticles as potential controlled release drug delivery systems. *J. Control. Rel.* 157, 168-182 (2012).
13. Fasano M, Curry S, Terreno E. The extraordinary ligand binding properties of human serum albumin. *IUBMB Life* 57, 787-796 (2005).

14. Duranton C, Tanneur V, Lang C. A High Specificity and Affinity Interaction with Serum Albumin Stimulates an Anion Conductance in Malaria-Infected Erythrocytes *Cell Physiol. Biochem.* 22, 395-404 (2008).
15. Tahir AE, Malhotra P, Chauhan VS. Uptake of proteins and degradation of human serum albumin by Plasmodium falciparum-infected human erythrocytes. *Malaria Journal* 2 (2003).
16. Krishna S, Ulhemann A, Haynes RK. Artemisinins: mechanisms of action and potential for resistance. *Drug Resistance Updates* 7, 233–244 (2004).
17. Artemether-Monographs of antimalarial drugs. *International Pharmacopoeia*, Third edition, WHO, Geneva, 5,187-190 (2003).
18. Yang YZ, Asawamahasakda W, Meshnick SR. Alkylation of human albumin by the antimalarial artemisinin. *Biochem. Pharmacol.* 46, 336-339 (1993).
19. Read M, Hyde JE. Simple *in vitro* culture of the malaria parasite *Plasmodium falciparum* (erythrocytic stages): suitable for large-scale preparations. In: *Protocols in Molecular Parasitology*. Hyde JE. (Ed.), 21, 43-55 (1993).
20. Langer K, Balthasar S, Vogel V, Dinauer N, Briesen H, Schubert D. Optimization of the preparation process for Human serum albumin (HSA) nanoparticles, *Int. J. Pharm.* 257, 169-180 (2003).
21. Weber C, Coester C, Kreuter J, Langer K. Desolvation process and surface characterisation of protein nanoparticles. *Int. J. Pharm.* 194, 91-102 (2000).
22. Jun JY, Nguyen HH, Paik S, Chun HS, Kang B, Ko S. Preparation of size-controlled bovine serum albumin (BSA) nanoparticles by modified desolvation method. *Food Chem.* 127, 1892-1898 (2011).
23. Watcharin W, Schmithals C, Pleli T. et al. Biodegradable human serum albumin nanoparticles as contrast agents for the detection of hepatocellular carcinoma by magnetic resonance imaging. *Eur. J. Pharm. Biopharm.* 87, 132–141 (2014).
24. Dubey RD, Alam N, Saneja A et al. Development and evaluation of folate functionalized albumin nanoparticles for targeted delivery of gemcitabine. *Int. J. Pharm.* 492, 80–91 (2015).

25. ICH Harmonised Tripartite Guideline, Pharmaceutical Development, Q8(R2) Current Step 4 version, dated August 2009.
26. Ibrahim N, Ibrahim H and Kim S. Interactions between antimalarial indolone-N-oxide derivatives and human serum albumin. *Biomacromolecules*, 11, 3341–3351 (2010).
27. Bian Q, Liu J, Tian J, Hu Z. Binding of genistein to human serum albumin demonstrated using tryptophan fluorescence quenching. *Int. J. Biol. Macromol.* 34, 275–279 (2004).
28. Sharma P, Sharma J. *In vitro* hemolysis of human erythrocytes— by plant extracts with antiplasmodial activity. *Ethnopharmacology* 74, 239–243 (2001).
29. Grennady Wirjanata,^a Boni F. Sebayang,^b Ferryanto Chalfein et al. Potent *Ex Vivo* Activity of Naphthoquine and Methylene Blue against Drug-Resistant Clinical Isolates of *Plasmodium falciparum* and *Plasmodium vivax* [Antimicrob Agents Chemother.](#) 59, 6117–6124 (2015).
30. Russell B, Chalfein F, Prasetyorini B. Determinants of *In Vitro* Drug Susceptibility Testing of *Plasmodium vivax* [Antimicrob Agents Chemother.](#) 52, 1040–1045 (2008).
31. Matthews H, Usman-Idris M, Khan F, Read M, Nirmalan N. Drug repositioning as a route to anti-malarial drug discovery: preliminary investigation of the *in vitro* anti-malarial efficacy of emetine dihydrochloride hydrate. *Malaria Journal* (12), 359-370 (2013).
32. Joshi M, Pathak S, Sharma S, Patravale V. Design and *in vivo* pharmacodynamic evaluation of nanostructured lipid carriers for parenteral delivery of artemether: Nanoject. . *Int. J. Pharm.* 364, 119-26 (2008).
33. Patil S , Joshi M Pathak S, Sharma S and Patravale V. Intravenous b-artemether formulation (ARM NLC) as a superior alternative to commercial artesunate formulation *J. Antimicrob. Chemother.* 67, 2713–2716 (2012).
34. Ibrahim N, Ibrahim H, Sabater AM, et al., Artemisinin nanoformulation suitable for

intravenous injection: Preparation, characterization and antimalarial activities
Int. J. Pharm., 495, 671-679 (2015).

35. Matar KM, Awad AI and Elamin SB. Pharmacokinetics of artesunate alone and in combination with sulfadoxine/pyrimethamine in healthy Sudanese volunteers
Am. J. Trop. Med. Hyg. 90(6),1087–1093 (2014).
36. Gad SC, Aubert N, Spainhour B, et al., Nonclinical Vehicle Use in Studies by Multiple Routes in Multiple Species. *International Journal of Toxicology*, 25,499–521 (2006).
37. César IDC, Nogueira FHA, Pianetti GA. Simultaneous determination of artemether and lumefantrine in fixed dose combination tablets by HPLC with UV detection. *J. Pharm. Biomed. Anal.* 48, 951–954 (2008).
38. Shena Z, Ma G, Dobashib T, Maki Y, Su Z. Preparation and characterization of thermo-responsive albumin nanospheres. . *Int. J. Pharm.* 346, 133–142 (2008). Wang YJ, Wang C, Gong CY, et al. Polysorbate 80 coated poly (ϵ -caprolactone)–poly (ethylene glycol)–poly (ϵ -caprolactone) micelles for paclitaxel delivery. *Int. J. Pharm.* 434, 1-8 (2012).
39. Ghosh P, Roy AS, Chaudhury S, et al. Preparation of albumin based nanoparticles for delivery of fisetin and evaluation of its cytotoxic activity. *Int J Biol Macromol.* 86, 408-17 (2016).
40. Langer K, Anhorn MG, Steinhauser I, et al. Human serum albumin (HSA) nanoparticles: Reproducibility of preparation process and kinetics of enzymatic degradation. *Int. J Pharm.* 347, 109-117 (2008).
41. Carter and Ho, 1994 D.C. Carter, J.X. Ho, Structure of serum albumin. *Adv. Protein Chem.* 45 153–203 (1994).

42. Dreisa S, Rothweilerb F, Michaelisb M, Cinatl Jr. J, Kreutera J, Langer K. Preparation, characterisation and maintenance of drug efficacy of doxorubicin-loaded human serum albumin (HSA) nanoparticles. *Int. J. Pharm.* 341, 207–214 (2007).
43. Desai N, Tao C. Protein Stabilized Pharmacologically Active agents, methods for the preparation thereof and methods for the use thereof. *United States Patent*, Patent No. US 6,749,868 B1 (2004).
44. Ibrahim N, Ibrahima H, Dormoic J, et al. Albumin-bound nanoparticles of practically water-insoluble antimalarial lead greatly enhance its efficacy. *Int. J. Pharm.* 464, 214–224 (2014).
45. Anhorn M, Mahler H, Langer K. Freeze drying of human serum albumin (HSA) nanoparticles with different excipients. *Int. J. Pharm.* 363, 162-169 (2008).
46. Chang, LL, Shepherd D, Sun, J, Ouellette, D, Grant, KL, Tang XC, Pikal MJ. Mechanism of protein stabilization by sugars during freeze-drying and storage: native structure preservation, specific interaction, and/or immobilization in a glassy matrix *J. Pharm. Sci.* 94, 1427–1444 (2005).
47. Trynda-Lemiesz L. Paclitaxel-HSA interaction. Binding sites on HSA molecule. *Bioorg. Med. Chem.* 12, 3269–75 (2004).
48. Gong G, Pan Q, Wang K, Wu R, Sun Y and Lu Y. Curcumin-incorporated albumin nanoparticles and its tumor image. *Nanotechnology* 26, 045603 (8pp) (2015).
49. Wan X, Zheng X, Pang X, Zhang Z, Zhang O. Incorporation of lapatinib into human serum albumin nanoparticles with enhanced anti-tumor effects in HER2-positive breast cancer. *Colloid Surface B.* 136, 817–827 (2015).
50. Yang Z, Gong W, Wang Z, et al. A novel drug-polyethylene glycol liquid compound method to prepare 10-hydroxycamptothecin loaded human serum albumin nanoparticle. *Int. J. Pharm.* 490, 412–428 (2015).
51. A. Bansal, D.N. Kapoor, R. Kapil, N. Chhabra, S. Dhawan. Design and development of paclitaxel-loaded bovin serum albumin nanoparticles for brain targeting. *Acta Pharm.* 61 141–156 (2011).
52. Kouchakzadeh Shojaosadati SA, Shokr F. Efficient loading and entrapment of tamoxifen in human serum albumin based nanoparticulate delivery system by a modified desolvation technique. *Chem. Eng. Res.Des.* 92, 681-1692 (2014).

53. Gholamreza DN, Khezaeli P, Rahmani P. Study of the effects of Polyethylene Glycol Sorbitan Esters Surfactants Group on Biological Membrane. *Int. J. Pharmacol.* 4 27-31 (2008).
54. Arora S, Rajwade J, Paknikar K. Nanotoxicology and in vitro studies: The need of the hour. *Toxicology and Applied Pharmacology* 258, 151-165 (2012).
55. Pereverzev E., Treschalin I, Bodyagin D, et.al. Influence of the formulation on the tolerance profile of nanoparticle-bound doxorubicin in healthy rats: focus on cardio- and testicular toxicity. *Int. J. Pharm.* 337, 346-56 (2007).
56. Tanariya P, Tippawangkoso P. *In vitro* sensitivity of *Plasmodium falciparum* and clinical response to lumefantrine (benflumetol) and artemether. *J. Clin. Pharmacol.* 49, 437-444 (2000).
57. Chambers E, Mitragotri S. Prolonged circulation of large polymeric nanoparticles by non-covalent adsorption on erythrocytes. *J. Control. Rel.* 100, 111-119 (2004).
58. Rothen-Rutishauser BSS, Haenni B, Kapp N, Gehr P. Interaction of fine particles and nanoparticles with red blood cells visualized with advanced microscopic techniques. *Environ. Sci Technol*, 40, 4353–4359, (2006).
59. Baniecki ML, Wirth DF, Clardy J. High-Throughput *Plasmodium falciparum* Growth Assay for Malaria Drug Discovery. *Antimicrob. Agents Chemother.* 51,716-723 (2007).
60. Aditya NP, Patankar S, Souto EB. Artemether-loaded lipid nanoparticles produced by modified thin-film hydration: Pharmacokinetics, toxicological and *in vivo* antimalarial activity. *Eur. J. Pharm. Sci.* 40, 448-455 (2010).
61. John CC, Kutamba E, Mugarura K, and Opoka RO. Adjunctive therapy for cerebral malaria and other severe forms of *Plasmodium falciparum* malaria *Expert Rev. Anti-Infective Therap.* 8, (2010).
62. Jain S, Basu H, Prabhu P, et al. Parasite impairment by targeting Plasmodium-infected RBCs using glyceryl-dilaurate nanostructured lipid carriers, *Biomaterials* 35, 6636-6645 (2014).
63. Teng Z, Luo Y, Wang Q. Nanoparticles synthesized from soy protein: preparation, characterization, and application for nutraceutical encapsulation. *J. Agric. Food Chem.* 60, 2712–2720 (2012).

64. Shegokar R, Singh KK, Müller RH. Production & stability of stavudine solid lipid nanoparticles—From lab to industrial scale. *Int. J. Pharm.* 416, 2461–470 (2011).
65. Abdelwahed H, Degobert G, Stainmesse S, Fessi H. Freeze-drying of nanoparticles: formulation, process and storage considerations. *Adv. Drug Deliv. Rev.* 58, 1688–1713 (2006).
66. Dadparvara M, Wagner S, Wienb S, et al. Freeze-drying of HI-6-loaded recombinant human serum albumin nanoparticles for improved storage stability. *Eur. J. Pharm. Biopharm.* 88, 510–517 (2014).
67. Han Y, Jin BS, Lee SB, Sohn J, Joung YJW, Lee JH. Effects of sugar additives on protein stability of recombinant human serum albumin during lyophilization and storage. *Arch. Pharm. Res.* 30, 1124–1131 (2007).
68. Wilson B, Ambika TV, Patel RD, Jenita JL, Priyadarshini SR. Nanoparticles based on albumin: preparation, characterization and the use for 5-fluorouracil delivery. *Int. J. Biol. Macromol.* 51, 874–878 (2012).
69. Wilson B, Lavanya Y, Priyadarshini SR et al., Albumin nanoparticles for the delivery of gabapentin: preparation, characterization and pharmacodynamic studies. *Int. J. Pharm.* 473, 73–79 (2014).
70. Wacker M. Nanocarriers for intravenous injection—The long hard road to the market. *Int. J. Pharm.* 457, 50–62 (2013).
71. Dubey RD, Alam N, Saneja A, et al. Development and evaluation of folate functionalized albumin nanoparticles for targeted delivery of gemcitabine. *Int. J. Pharm.* 492, 80–91 (2015).
72. Haldar K, Uyetake L. The movement of fluorescent endocytic tracers in Plasmodium falciparum infected erythrocytes. *Mol. Biochem. Parasitol.* 50, 161–177 (1992).
73. Pouvelle B, Gormley JA, Taraschi TF. Characterization of trafficking pathways and membrane genesis in malaria-infected erythrocytes. *Mol. Biochem. Parasitol.* 66, 83–96 (1994).
74. Burns ER, Pollack SP. falciparum infected erythrocytes are capable of endocytosis, *In Vitro Cell Dev. Biol.* 24, 481–486 (1988).

75. Ginsburg H and Stein, WD. Biophysical analysis of novel transport pathways induced in red blood cell membranes. *Mol. Biochem. Parasitol.* 96, 1-10 (1987).
76. Yuthavong Y, Wilairat P, Panijpan B, Potiwan C, et al. Alteration in membrane proteins of mouse erythrocytes infected with different species and strains of malaria parasites *Comp. Biochem. Physiol.* 63B, 83–85. (1979).
77. Ginsburg H and Stein WD, The New Permeability Pathways Induced by the Malaria Parasite in the Membrane of the Infected Erythrocyte: Comparison of Results Using Different Experimental Techniques *J. Membr. Biol.* 197, 113-134 (2004).
78. Lauer SA, Rathod PK, Ghori N, Haldar K. A membrane network for nutrient import in red cells infected with the malaria parasite *Science* 276, 1122–112 (1997).
79. Haldar K. Ducts, Channels and Transporters in *Plasmodium*-infected Erythrocytes. *Parasitol. Today*, 10, 393-395 (1994).
80. Deponte, M, Hoppe HC, Lee MCS, et al. Przyborski, Wherever I may roam: Protein and membrane trafficking in *P. falciparum*-infected red blood cells. *Mol. Biochem. Parasitol.*, 186, 95-116 (2012).
81. Saliba KJ, Kirk SK. Nutrient acquisition by intracellular apicomplexan parasites: staying in for dinner. *Int. J. Parasitol.* 31, 1321–1330 (2001).
82. Olliaro P, Castelli F. *Plasmodium falciparum*: an electronmicroscopy study of caveolae and trafficking between the parasite and the extracellular medium. *Int. J. Parasitol.* 27, 1007–1012 (1997).
83. Asahi H. *Plasmodium falciparum*: Chemically defined medium for continuous intraerythrocytic growth using lipids and recombinant albumin *Exp. Parasitol.* 121, 22-28 (2009).
84. Asahia H, Kanazawab T, Hirayamac N, Kajiharad Y. Investigating serum factors promoting erythrocytic growth of *Plasmodium falciparum*. *Exp. Parasitol.* 7–15 (2005).
85. Pouvelle B, Gysin J. Presence of the parasitophorous duct in *Plasmodium falciparum* and *P. vivax* parasitized Saimiri monkey red blood cells. *Parasitol. Today* 13, 357–361 (1997).
86. Bodammer JE, Bahr GF. The initiation of a "metabolic window" in the surface of host erythrocytes by *Plasmodium berghei* NYU-2. *Lab Invest.* 28, 708–18 (1973).

87. Hasan GM, Garg N, Dogra E, Surolia R, Ghosh PC. Inhibition of the Growth of *Plasmodium falciparum* in Culture by Stearylamine-Phosphatidylcholine Liposomes. *J. Parasitol. Res.* 2011 (2011).
88. Urbán P, Estelrich J, Cortés A, Fernández-Busquets X. A nanovector with complete discrimination for targeted delivery to *Plasmodium falciparum*-infected versus non-infected red blood cells *in vitro*. *J. Control. Rel.* 151, 202–211(2011).
89. Movellan J, Urbán P, Moles E. Amphiphilic dendritic derivatives as nanocarriers for the targeted delivery of antimalarial drugs, *Biomaterials* 35, 7940-7950 (2014).

Executive Summary

- Biodegradable artemether (ATM) loaded human serum albumin (HSA) based nanoparticles (AAN) successfully developed as an intravenous drug delivery system for the treatment of malaria. Robust formulation optimised for critical product and process parameters with reproducible particle size (<100nm) and high entrapment efficiency.
- Complete characterisation carried out in terms morphology, particle size, polydispersity index (PI), zeta potential, differential scanning calorimetry (DSC), X-ray diffraction (XRD), Fourier transform infrared spectroscopy (FTIR) and, *in-vitro* drug release
- Fluorescence spectroscopy demonstrated binding of drug with HSA in the nanoparticulate formulation as seen by decrease in the fluorescence intensity in the spectra of AAN nanoparticles in comparison with the blank HSA nanoparticles
- *In vitro* erythrocyte toxicity study established the safety for intravenous administration of AAN.
- Selective internalisation of AAN into *Plasmodium*-infected RBCs (pRBCs) in preference to non-infected erythrocytes was observed using confocal imaging.
- *In vitro* susceptibility studies with *Plasmodium falciparum* showed 50% dose reduction for AAN as compared to drug-only controls to achieve IC₅₀ levels of inhibition.
- The nanoparticles exhibited 2-fold higher peak drug concentrations in RBCs with antimalarial activity at 50% of therapeutic doses in *Plasmodium. bergeri*-infected mice.

- HSA-based nanoparticles could offer a safe and effective approach for selective targeting of antimalarial drugs *Plasmodium* infected cells. To best of our knowledge this the first report of selective targeting of pRBCs with HSA based nanoparticles.

Table 1: Risk assessment for control of critical quality attributes for fabricating HSA nanoparticles

Risk assessment related to		Critical Quality Attributes			
		Particle size	Polydispersity index	Drug entrapment	Stability
Materials	HSA concentration	High	High	High	Medium
	Drug: HSA ratio	Medium	Medium	High	Low
	Solvent concentration	High	High	Low	Medium
	Surfactant concentration	Medium	Medium	High	High
Process	Homogenization pressure	High	High	Medium	High
	Homogenization cycles	Medium	Medium	Medium	Medium
Environment	pH	High	High	Low	Medium
	Cryoprotectant	High	High	Low	Medium

Table: 2 Concentration levels of the dependent variables in factorial designs

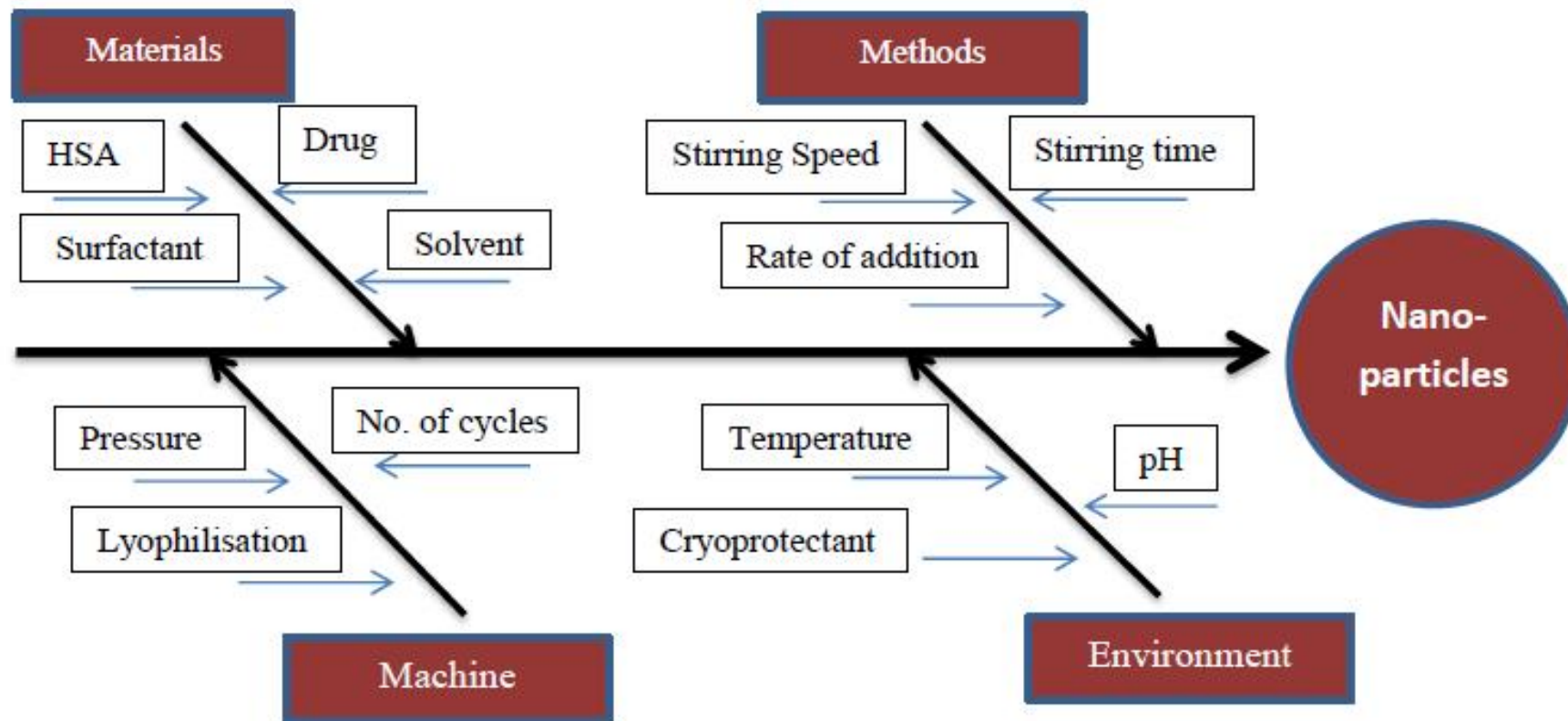
Factors	Factorial levels		
	-1	0	+1
HSA (%w/v)	1	2	3
Solvent (%v/v)	20	30	40
Polysorbate 80 (%w/v)	3	5	7

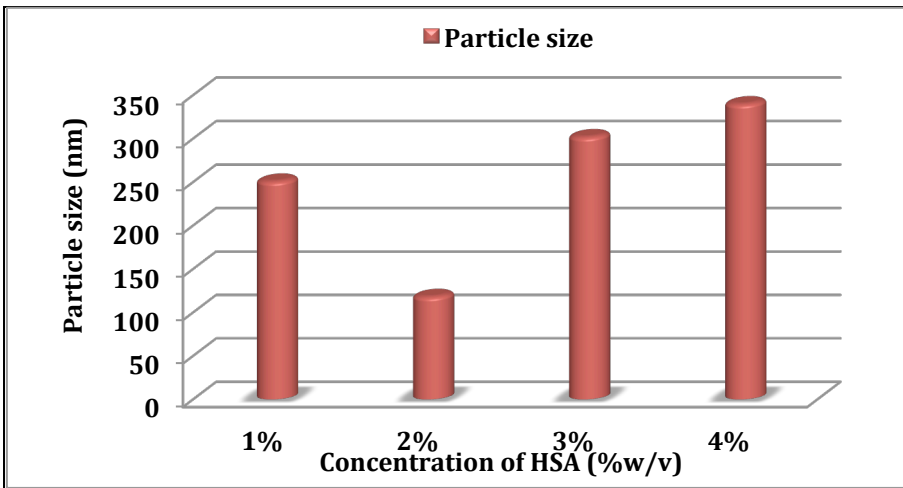
Table 3: Optimisation of Drug: HSA ratio

Drug: HSA ratio	Particle size (nm)	Poly dispersity index	Observations	Entrapment efficiency (%)
1:20	230.6	0.348	Good drug dispersion	68.45
1:10	85.5	0.121	Good drug dispersion	77.56
1:5	-		Precipitation of the drug	-

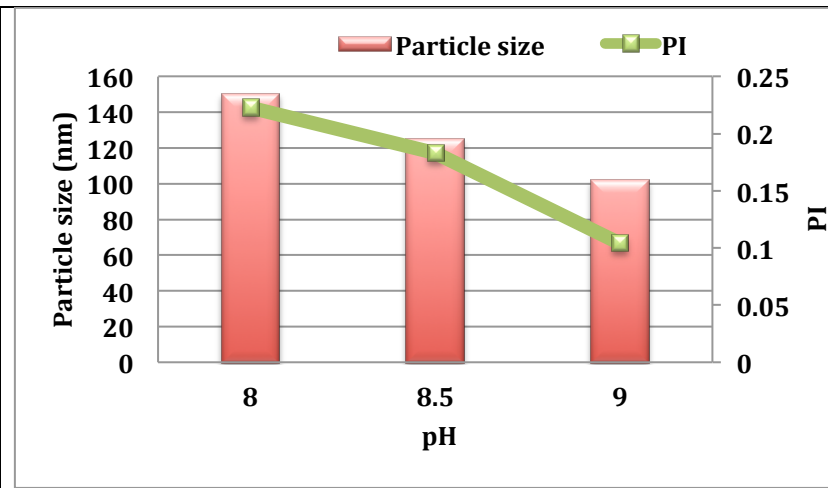
Table 4: Number of *P. Berghei* infected mice surviving in each group at the end of 30th day (n=5)

Treatment	Number of animals survived	% Survival
Untreated Group	0/5	0
AAN (0.624mg/day;100% dose)	3/5	60
AAN (0.312mg/day;50% dose)	3/5	60

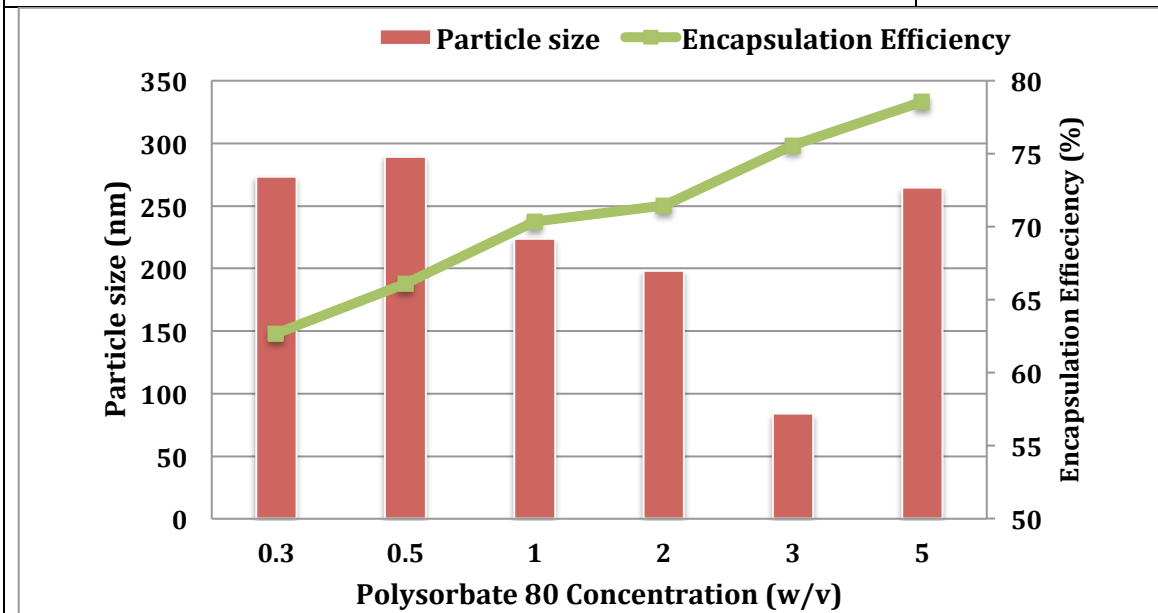




(a)



(b)



(c)

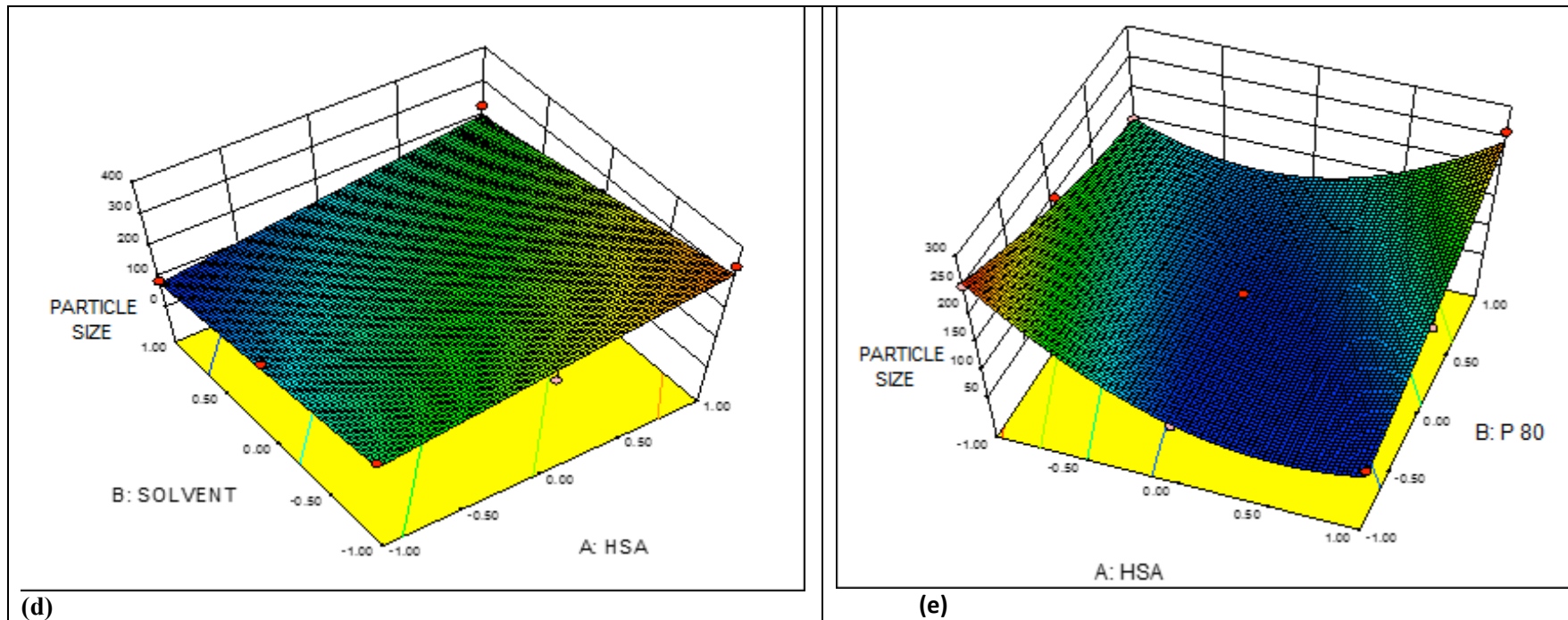


Figure 2: Optimization of HSA nanoparticles (a) Effect of HSA concentration on particle size of nanoparticles (b) Effect of pH on particle size and polydispersity index of nanoparticles (c) Effect of polysorbate 80 concentration on particle size and encapsulation efficiency of nanoparticles (d) 3-D Response surface plot showing the influence of HSA and solvent concentration on particle size of nanoparticles (e) 3-D Response surface plot showing the influence of HSA and polysorbate 80 concentration on particle size of nanoparticles. HSA: Human serum albumin, P 80: Polysorbate 80

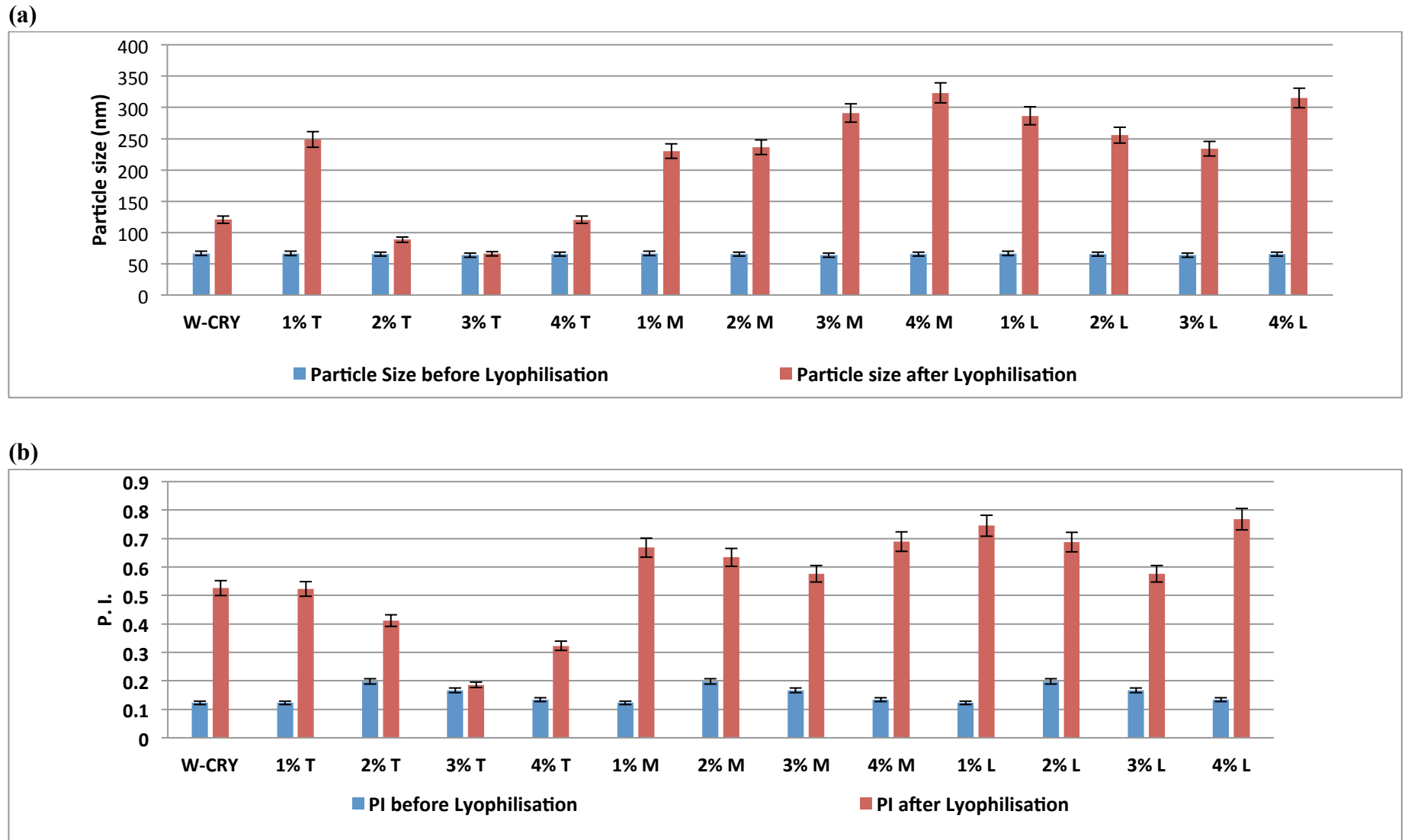


Fig 3: Effect of Cryoprotectants on the (a) mean article size before and after lyophilisation and (b) Polydispersity index before and after lyophilisation of AAN (mean \pm SD, $n = 3$). W-CRY: Without cryoprotectant; T: Trehelose; M: Mannitol; L:Lactose

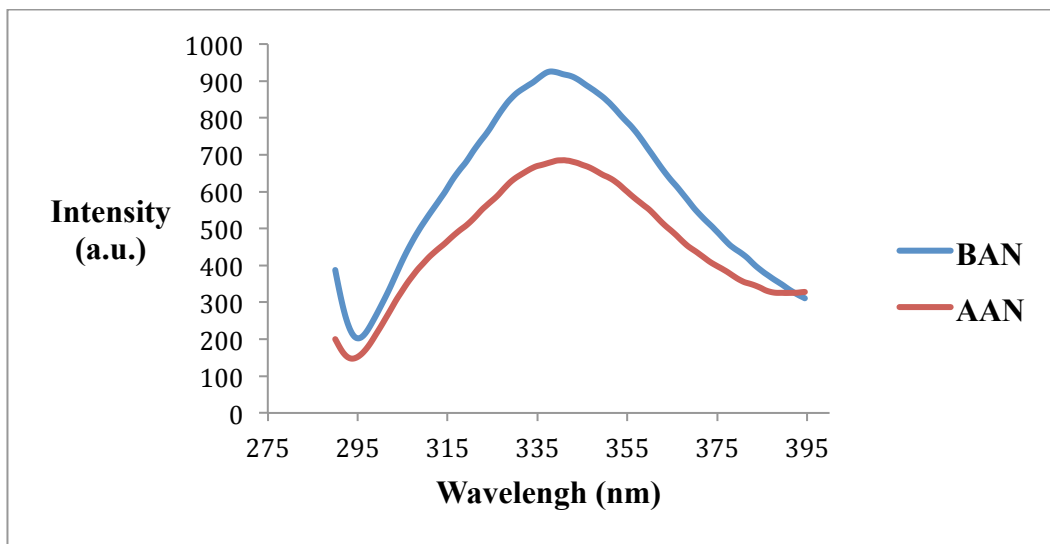
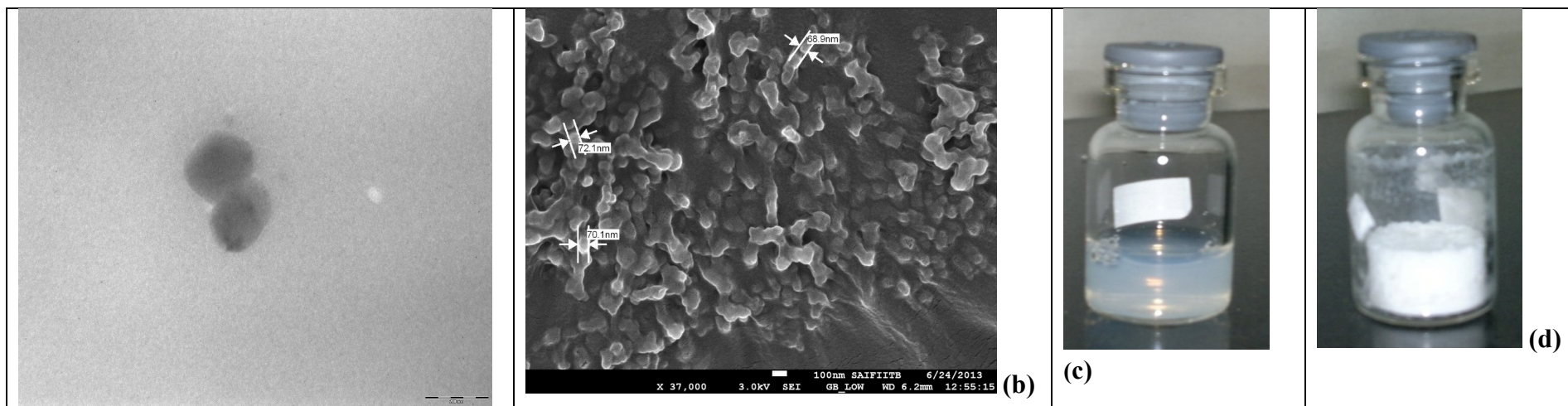


Fig 4: Fluorescence emission spectra of AAN and BAN following excitation at 280nm
AAN: Artemether loaded HSA nanoparticle, BAN: blank nanoparticle with HSA only.



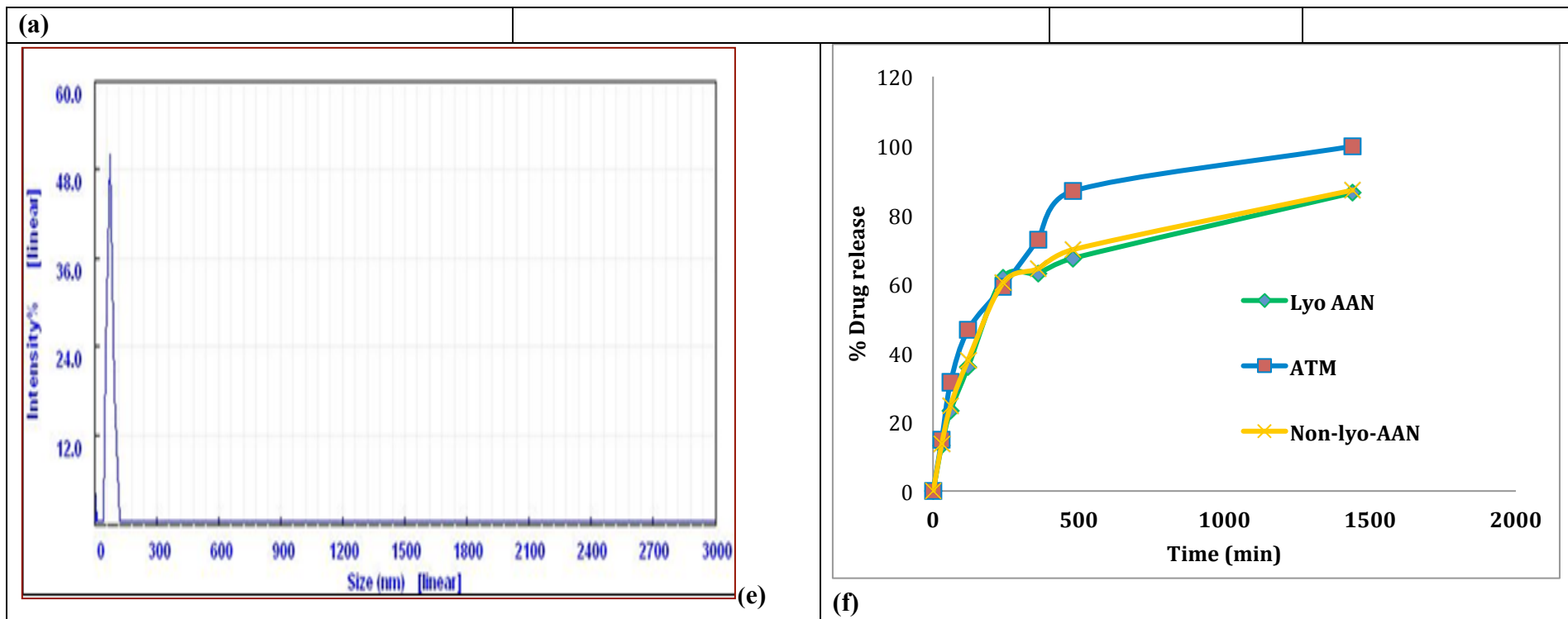


Figure 5: Characterization of AAN: (a) Transmission electron microscopic image of AAN (b) Scanning electron microscopic image of AAN (c) Photograph of AAN before lyophilisation (d) Photograph of AAN after lyophilisation (e) Representation of particle size distribution by intensity using photon correlation spectroscopy (f) *In-vitro* release profile of lyophilised and non lyophilised AAN in PBS: Ethanol 50:50 v/v at 37⁰ C (mean ± SD, n = 3)

Lyo AAN: Lyophilised artemether loaded HSA nanoparticle, Non lyo-AAN: Artemether loaded HSA nanoparticles prior to lyophilisation

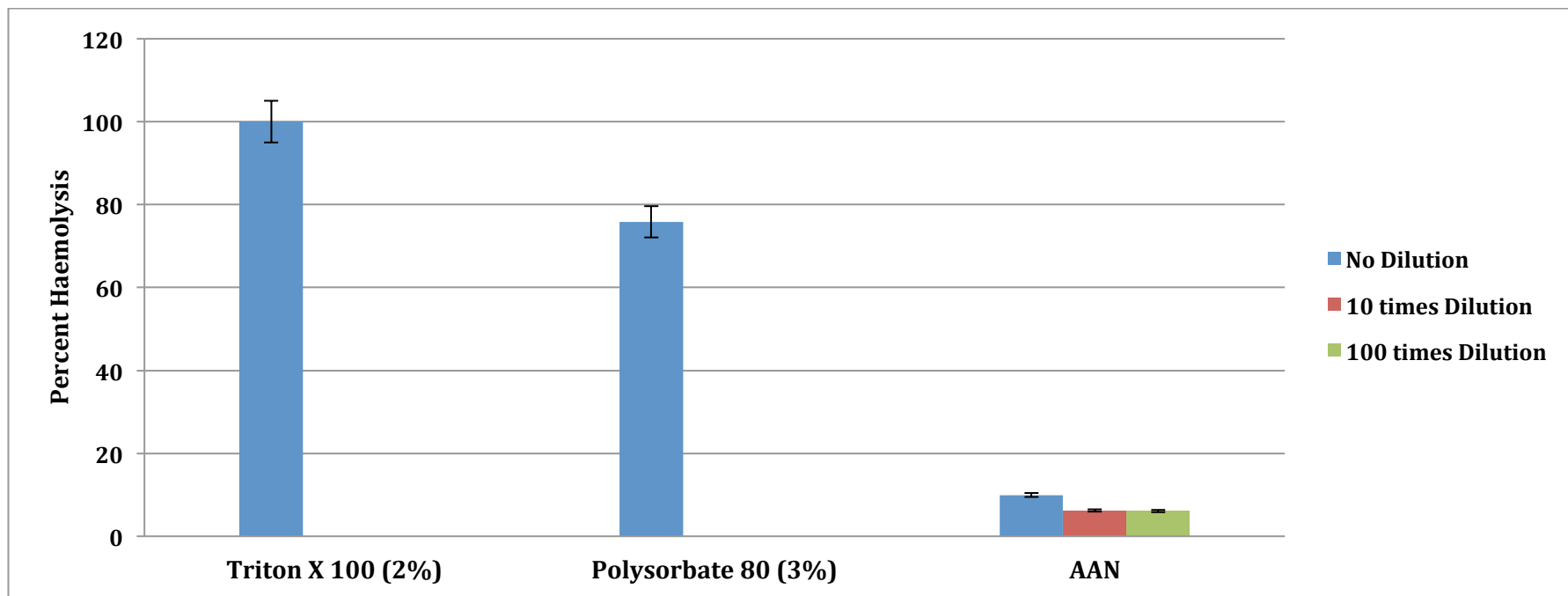


Figure 6: *In vitro* erythrocyte haemolysis after treatment with varying dilutions AAN in normal saline (mean \pm SD, $n = 3$)
AAN: Artemether HSA nanoparticles; Triton X 100 (2%) in normal saline as positive control; Polysorbate 80 (3%) in normal saline as reference

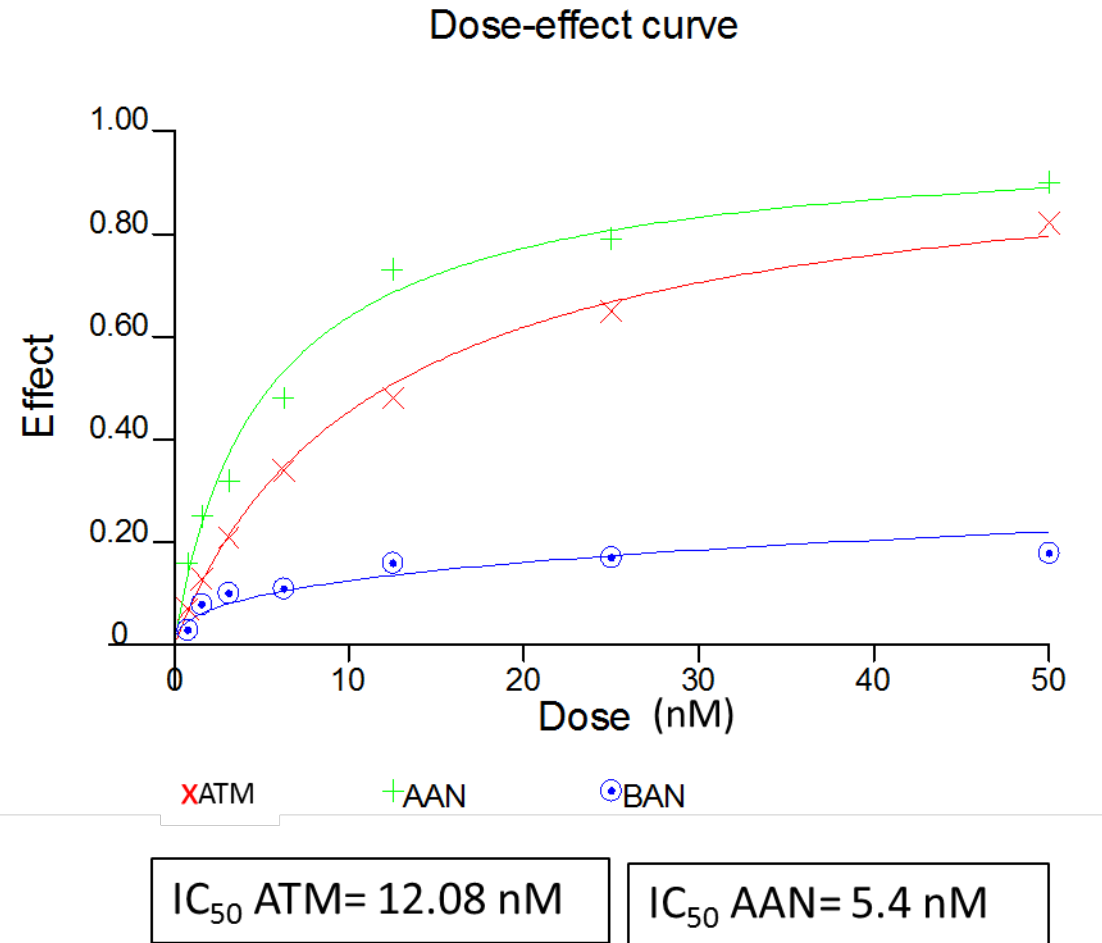
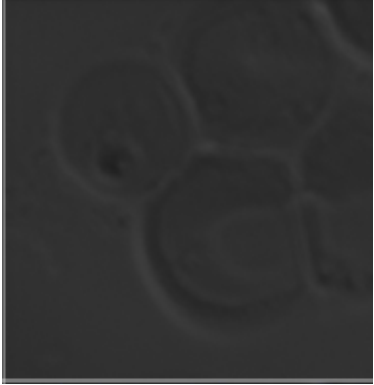
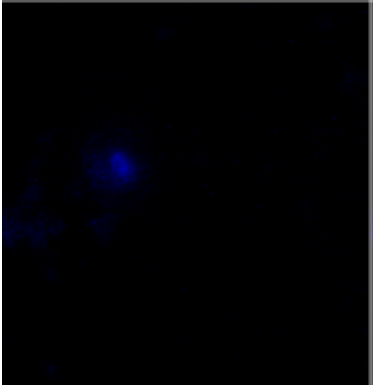
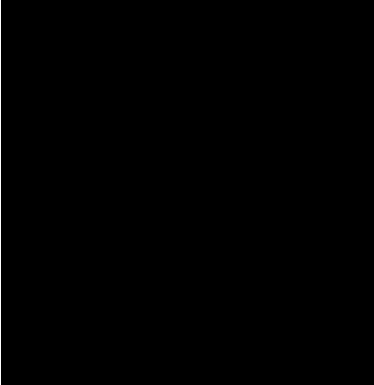
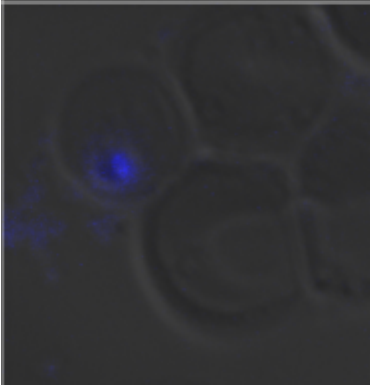
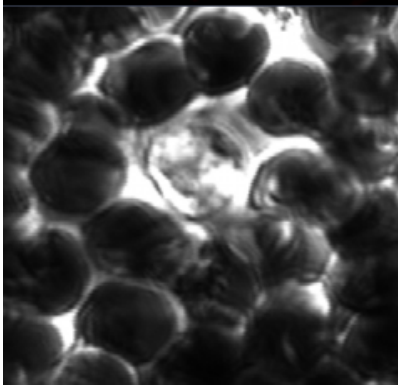
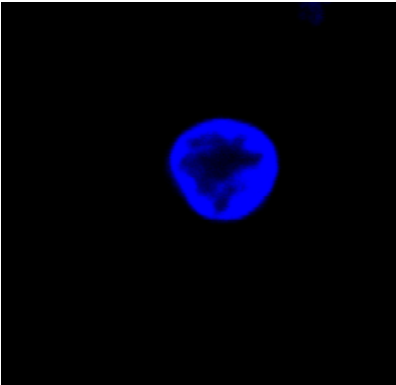
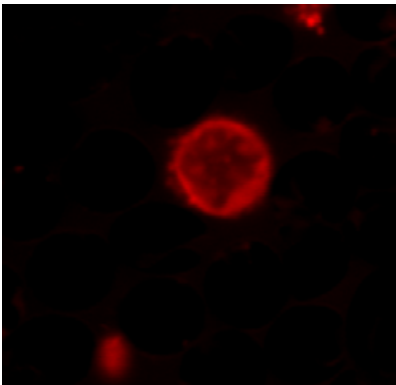
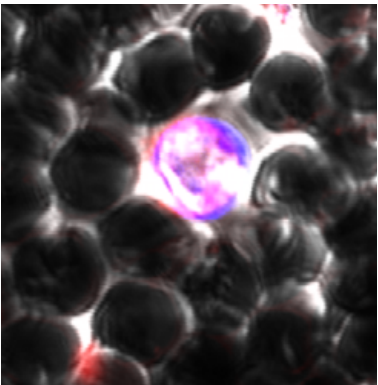
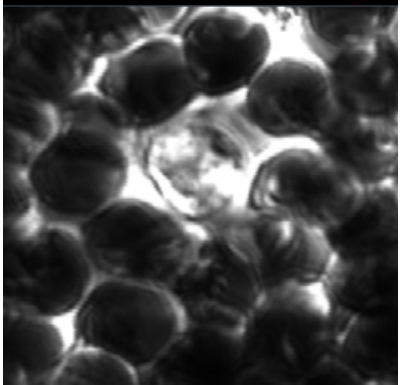
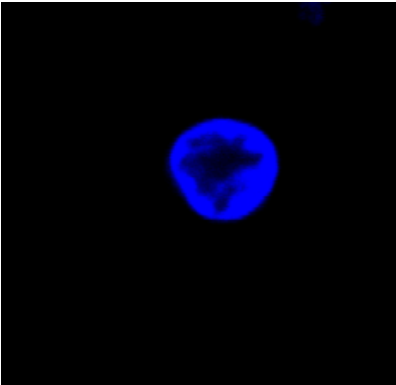
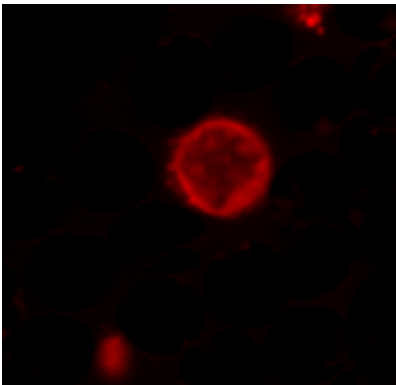
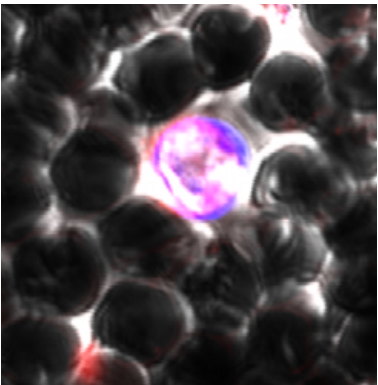


Figure 7. Dose response curves depicting mean parasitaemia inhibition vs. drug concentration 48 hours after incubation *in-vitro* (mean \pm SD, n = 3). ATM: artemether drug only, AAN: Artemether loaded HSA nanoparticle, BAN: blank nanoparticle with HSA only.

Time	Bright field image	DAPI	Rhodamine B labelled AAN	Merged
<p>ed RBC stained DAPI while non ed is not stained</p>				
<p>ected and non ected RBC co- re incubated Rhodamine belled AAN</p>				
<p>5 minutes</p>				

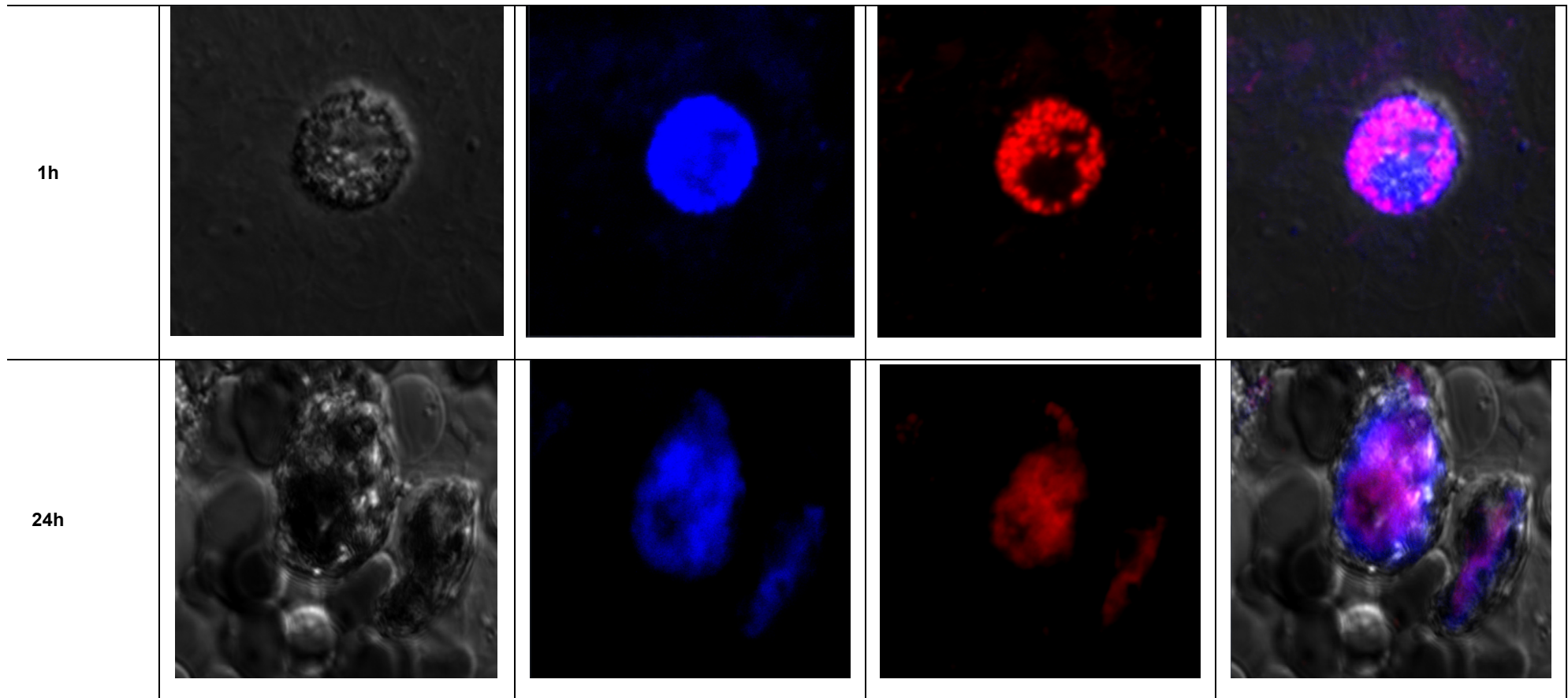


Figure 8: Confocal images showing selective targeting of rhodamine labelled nanoparticles to pRBCs vs. RBCs. Rhodamine labelled nanoparticles were added to living co-cultures of *P. falciparum*-infected RBCs and non infected RBCs and incubated for the indicated times before sample preparation for microscopic analysis. Blue and red fluorescence represent DAPI (pRBC) and Rhodamine B (localization of AAN), respectively
Figure panels L to R bright field image, DAPI stained Plasmodium nucleus to indicate pRBC, Rhodamine labelled AAN and merged images

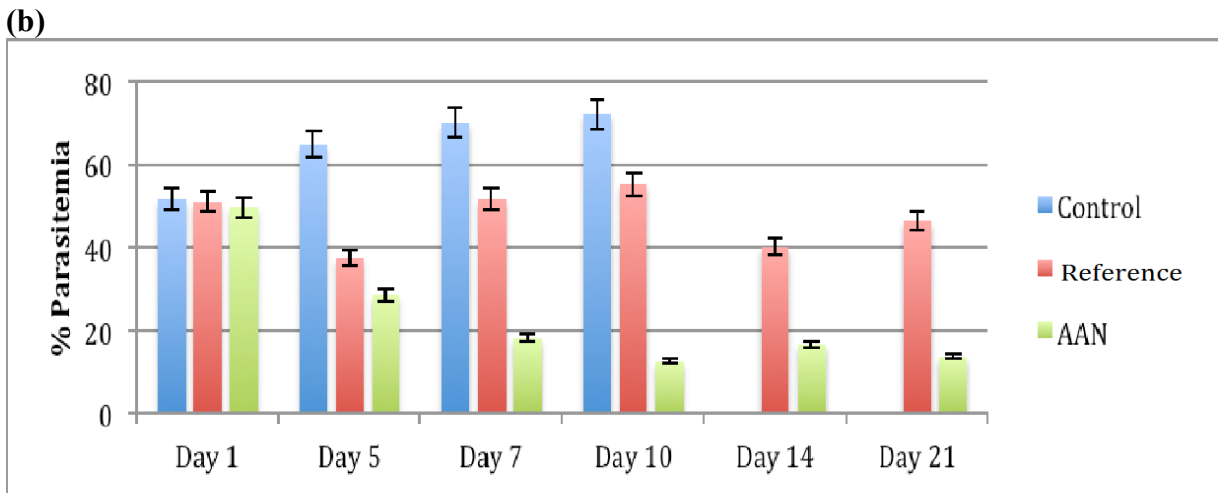
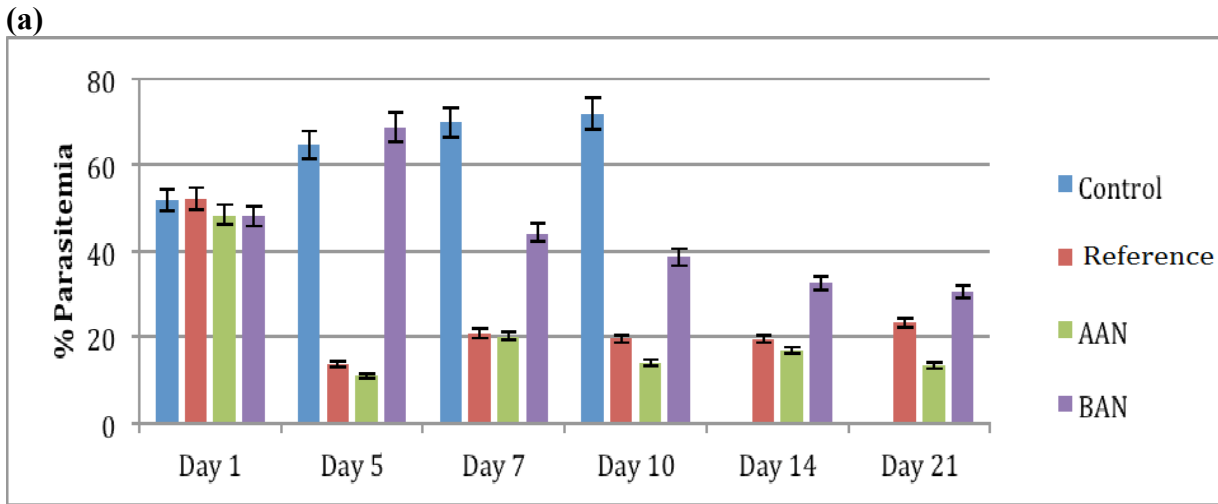


Figure 9: Mean percent parasitemia in suppressive test against *P. berghei* infected mice after treatment with AAN, BAN and Reference at (a) 100% (b) 50% dose levels, AAN: Artemether loaded HSA nanoparticle, BAN: blank nanoparticle with HSA only, Reference: Larinate artesunate marketed injection (Values are expressed as mean \pm SD n = 5 mice per group)

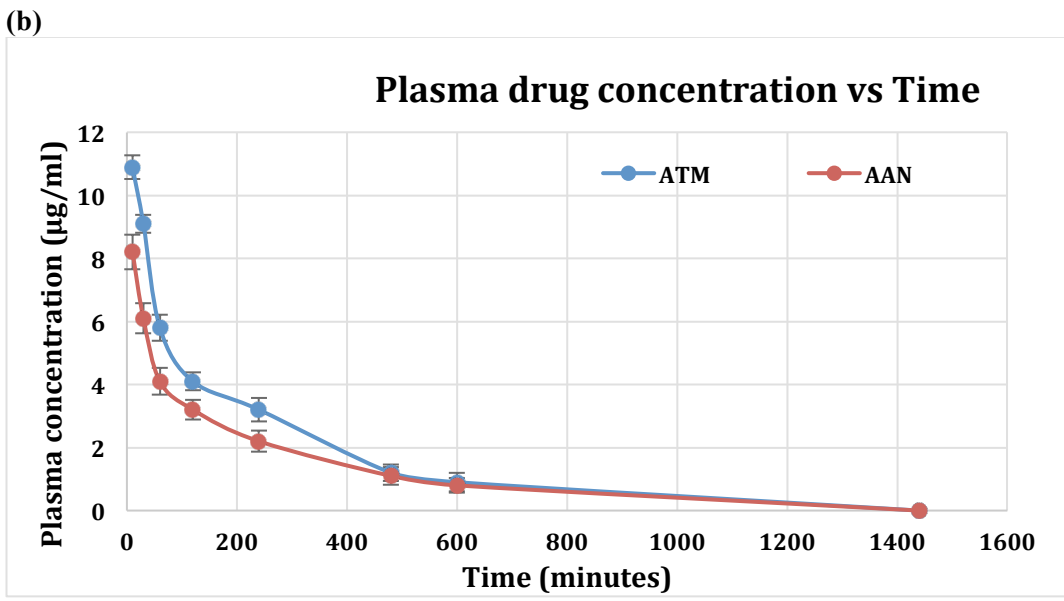
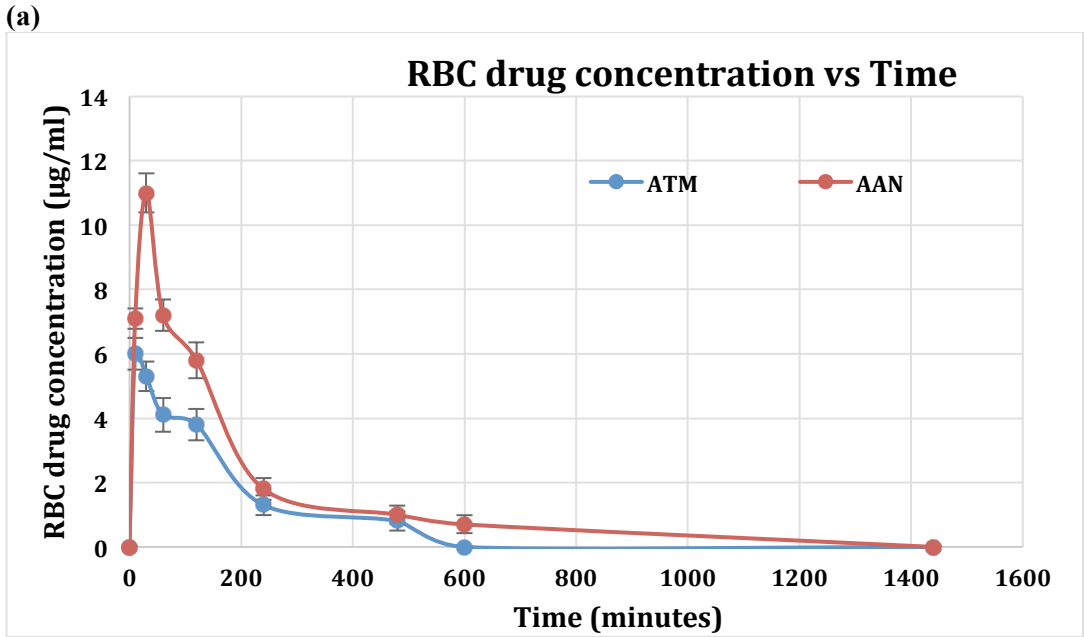


Figure 10: Drug concentration- time profiles in parasitized mice (a) RBC (b) Plasma (mean \pm SD, $n = 6$)